NAVAL POSTGRADUATE SCHOOL

MONTEREY, CALIFORNIA

THESIS

DEPTH ANALYSIS OF MIDWAY ATOLL USING QUICKBIRD MULTI-SPECTRAL IMAGING OVER VARIABLE SUBSTRATES

by

Mark A. Camacho

September 2006

Thesis Advisor:	Daria Siciliano
Co-advisor:	Richard C. Olsen

Approved for public release; distribution is unlimited

THIS PAGE INTENTIONALLY LEFT BLANK

REPORT DOCUMENTATION PAGE			Form Approved OMB No. 0704-0188

1. AGENCY USE ONLY *(Leave blank)*	2. REPORT DATE September 2006	3. REPORT TYPE AND DATES COVERED Master's Thesis

4. TITLE AND SUBTITLE Depth Analysis of Midway Atoll using QuickBird Multi-Spectral Imaging over Variable Substrates.	5. FUNDING NUMBERS
6. AUTHOR(S) Mark A. Camacho	
7. PERFORMING ORGANIZATION NAME(S) AND ADDRESS(ES) Naval Postgraduate School Monterey, CA 93943-5000	8. PERFORMING ORGANIZATION REPORT NUMBER
9. SPONSORING /MONITORING AGENCY NAME(S) AND ADDRESS(ES) N/A	10. SPONSORING/MONITORING AGENCY REPORT NUMBER

11. SUPPLEMENTARY NOTES The views expressed in this thesis are those of the author and do not reflect the official policy or position of the Department of Defense or the U.S. Government.

12a. DISTRIBUTION / AVAILABILITY STATEMENT Approved for public release; distribution is unlimited.	12b. DISTRIBUTION CODE A

13. ABSTRACT (maximum 200 words)

Shallow water bathymetry is important for both safe navigation and natural resource management purposes. Extracting depth information from spectral imagery allows identification of benthic features and characterization of coral reef habitats, especially in remote islands. Techniques have been developed to extract water depth from multispectral imagery (Lyzenga, 1978; Philpot, 1989). These techniques can be difficult to apply in optically shallow waters with heterogeneous bottom types and varying albedo, and require tuning of multiple parameters. An improved algorithm to extract water depth from multispectral satellite imagery was proposed by Stumpf et al. (2003) to generate bathymetric maps with limited *a priori* information. The algorithm is based on the ratios of transformed reflectance values in the visible bands, retrieving greater depths than previous algorithms and compensating for variable bottom type and albedo. This method requires fewer tunable parameters and can be applied to low-albedo features. Although Stumpf et al. (2003) conclude that the method is robust and works well over variable bottom types, recent studies have pointed out limitations, mostly attributable to varying albedo (Clark, 2005; Densham, 2005). This research attempts to quantify the contribution of variable benthic substrates to the algorithm's accuracy by classifying the scene into its main bottom types and tuning the coefficients separately. The algorithm is evaluated using a QuickBird high resolution multispectral image of the remote Midway Atoll, in the Northwestern Hawaiian Islands. Classifying the image into two main bottom types and tuning the coefficients separately produced a small improvement in the accuracy of the bathymetric estimates when bottom reflectance is included as a factor. This result indicates that Stumpf et al. (2003)'s ratio method is not insensitive to variable bottom type, and that knowledge of the distribution and extent of different benthic substrates in optically shallow waters has the potential to improve bathymetric derivation in remote coastal areas such as coral reef environments in the Pacific.

14. SUBJECT TERMS Bathymetry, QuickBird, ENVI, Ratio Algorithm, Remote Sensing, Satellite, Multi-Spectral, IKONOS, Midway Atoll, Coral Reefs.	15. NUMBER OF PAGES 91
	16. PRICE CODE

17. SECURITY CLASSIFICATION OF REPORT	18. SECURITY CLASSIFICATION OF THIS PAGE	19. SECURITY CLASSIFICATION OF ABSTRACT	20. LIMITATION OF ABSTRACT
Unclassified	Unclassified	Unclassified	UL

NSN 7540-01-280-5500 Standard Form 298 (Rev. 2-89)
Prescribed by ANSI Std. 239-18

THIS PAGE INTENTIONALLY LEFT BLANK

Approved for public release; distribution is unlimited

DEPTH ANALYSIS OF MIDWAY ATOLL USING QUICKBIRD MULTI-SPECTRAL IMAGING OVER VARIABLE SUBSTRATES

Mark A. Camacho
Lieutenant, United States Naval Reserve
B.S., United States Naval Academy, 2000

Submitted in partial fulfillment of the
requirements for the degree of

MASTER OF SCIENCE IN SPACE SYSTEMS OPERATIONS

from the

NAVAL POSTGRADUATE SCHOOL
September 2006

Author: Mark A. Camacho

Approved by: Dr. Daria Siciliano
Thesis Advisor

Dr. Richard C. Olsen
Co-Advisor

Dr. Rudolf Panholzer
Chairman, Space Systems Academic Group

THIS PAGE INTENTIONALLY LEFT BLANK

ABSTRACT

Shallow water bathymetry is important for both safe navigation and natural resource management purposes. Extracting depth information from spectral imagery allows identification of benthic features and characterization of coral reef habitats, especially in remote islands. Techniques have been developed to extract water depth from multispectral imagery (Lyzenga, 1978; Philpot, 1989). These techniques can be difficult to apply in optically shallow waters with heterogeneous bottom types and varying albedo, and require tuning of multiple parameters. An improved algorithm to extract water depth from multispectral satellite imagery was proposed by Stumpf et al. (2003) to generate bathymetric maps with limited *a priori* information. The algorithm is based on the ratios of transformed reflectance values in the visible bands, retrieving greater depths than previous algorithms and compensating for variable bottom type and albedo. This method requires fewer tunable parameters and can be applied to low-albedo features. Although Stumpf et al. (2003) conclude that the method is robust and works well over variable bottom types, recent studies have pointed out limitations, mostly attributable to varying albedo (Clark, 2005; Densham, 2005). This research attempts to quantify the contribution of variable benthic substrates to the algorithm's accuracy by classifying the scene into its main bottom types and tuning the coefficients separately. The algorithm is evaluated using a QuickBird high resolution multispectral image of the remote Midway Atoll, in the Northwestern Hawaiian Islands. Classifying the image into two main bottom types and tuning the coefficients separately produced a small improvement in the accuracy of the bathymetric estimates when bottom reflectance is included as a factor. This result indicates that Stumpf et al. (2003)'s ratio method is not insensitive to variable bottom type, and that knowledge of the distribution and extent of different benthic substrates in optically shallow waters has the potential to improve bathymetric derivation in remote coastal areas such as coral reef environments in the Pacific.

THIS PAGE INTENTIONALLY LEFT BLANK

TABLE OF CONTENTS

LIST OF FIGURES

LIST OF TABLES

THIS PAGE INTENTIONALLY LEFT BLANK

ACKNOWLEDGMENTS

I would like to first and foremost thank my wife Jill for all her encouragement and support throughout this thesis process. I wish to gratefully thank Dr. Daria Siciliano for guiding me through this thesis process and providing her expert knowledge to my thesis. Thank you for providing me with thoughtful guidance, expert advice, and patience. I would also like to thank Dr. Richard C. Olsen for this truly unique opportunity, great classroom teaching, and sponsorship. A special recognition is owed to Mr. Barry Christenson and his great staff at Midway Atoll. This thesis would not have been possible without their great support and enthusiasm to work with students from the Naval Postgraduate School. I would also like to thank Angela Puetz for all of her assistance and eagerness to help no matter how trivial my request or question. I can never express my appreciation to LCDR Randy Blankenship for all his assistance, great diving adventures, and friendship throughout our time at the Naval Postgraduate School.

THIS PAGE INTENTIONALLY LEFT BLANK

I. INTRODUCTION

A. PURPOSE OF RESEARCH

This research focuses on bathymetric mapping techniques in remote islands using satellite-deployed spectral imagery. Remote sensing from satellite platforms continues to be an essential tool to measure and study terrestrial, atmospheric, and oceanic properties. Spectral imagery of marine environments collected from satellite platforms has been used to augment current navigational charts (Busheuv, 1991; Chauhan, 2005), study coral reef features (Mumby, 2002; Lubin, 2001), monitor the health of coastal vegetation (Green et al., 2000; Kogan, 2001), and study ocean surface characteristics (Barton, 1995). The routine availability of information from satellite sensors has greatly bolstered the advancement of habitat mapping techniques and capabilities, including bathymetric derivation. Determination of water depth using traditional ship-based techniques has been disproportionately concentrated to areas that encompass high marine traffic, densely populated regions, and that are typically easy to access. Portions of the ocean that are remote and isolated have been spared extensive bathymetric mapping, typically due to high costs and logistics. Satellite-based remote sensing can remedy this problem by providing data on remote locations that would otherwise be hard to reach by ship or airborne sensors. Bathymetric information from remote Pacific islands and atolls is required for safe navigation and for monitoring benthic marine resources (Mumby, 2002; Stumpf et al., 2003). Although measuring the ocean from space is only one of many applications for optical remote sensing, this field is rapidly evolving and has been effectively used in shallow marine environments to determine water depths, identify benthic substrates, and estimate the biomass of submerged vegetation (Green et al., 2000).

Some of the early methods of mapping bathymetry were conducted using instruments mounted on glass-bottom boats or aircraft to analyze ocean radiances (Duntley, 1963). Other techniques ranged from basic aerial photography (Tewinkel, 1963) to more advanced analysis of multispectral satellite images (Polcyn, 1973; Weidmark, 1981). Bathymetry derivation from spectral imagery has been pursued for over five decades now by numerous researchers, among them Tewinkel (1963), Duntley

(1963), Rosenshein (1977), Philpot (1989), Maritorena (1994). In particular, a seminal paper by Lyzenga (1978) presented an empirical method to extract water depth and bottom type information. Lyzenga provided the foundation for subsequent algorithms and is still widely cited in the optical oceanography literature. Stumpf et al., (2003) expanded on Lyzenga's (1978) original water depth derivation. Stumpf et al. (2003) proposed an algorithm that uses a ratio of reflectances (hereby referred to as the "ratio method") claiming that it retrieves accurate depths over variable bottom types and low-albedo environments.

While the spatial resolution of traditional satellite-deployed optical sensors such as LANDSAT is often not sufficient for navigational use or fine-scale benthic classifications of ocean environments, the advent of high resolution (2-4m), multispectral satellite imagery has allowed higher accuracy in deriving water depth, mapping coral reefs benthic features, and study other ecological properties of marine environments. This shift first occurred in 1999 with the launch of IKONOS 2 by Space Imaging, which sent into orbit the first commercial 4-meter, multispectral imager. In 2002, the QuickBird satellite was launched by DigitalGlobe, providing an improved 2.4 meter field-of-view for multispectral and sub-meter resolution for panchromatic imagery. The increased spatial resolution makes it possible to better discriminate benthic substrates, improve water depth derivation, and obtain marine habitat maps with higher accuracy (Mumby 2002).

B. SPECIFIC OBJECTIVES

The objective of this study is to test the potential of deriving bathymetry over variable substrates at Midway Atoll, Northwestern Hawaiian Islands, using QuickBird multispectral imagery. In particular, building on work by Clark (2005) and Stumpf et al. (2003), this work will:

1) Use a QuickBird multispectral image to categorize benthic substrates at Midway Atoll based on their spectral characteristics, and groundtruth data collected *in situ*

2) Use the ratio method to extract depth separately over these variable substrates

3) Compare the bathymetric results derived over separate bottom types with bathymetric results derived over the whole image (irrespective of bottom type)

The motivation for this work originates from a limitation pointed out by Clark (2005) who found the ratio method for bathymetry derivation is altered by varying albedos and produces inaccurate results for different substrates. Clark (2005) suggested that the accuracy of the ratio method might be improved through pre-classification of bottom substrate. Using the 2004 QuickBird satellite image acquisition for Midway Atoll, this hypothesis will be tested by classifying the scene into the main bottom types, and tuning the bathymetry separately for each class.

A previous data collection of Midway Atoll was conducted with the IKONOS multispectral imager (4m pixel resolution) in 2000. The 2004 QuickBird multi-spectral image used in this study provides an almost two-fold increase in spatial resolution (2.4m), affording the additional benefit of obtaining more detailed bathymetric information for Midway Atoll than is currently available.

THIS PAGE INTENTIONALLY LEFT BLANK

II. PRINCIPLES OF RADIATIVE TRANSFER IN THE OCEAN AND ATMOSPHERE

Optical remote sensing is playing an increasingly important role in assessing and monitoring marine environments. It is important to understand the principles of light, its transmission through different mediums, and the optical systems designed to collect the imagery. In passive remote sensing, the sensor detects incoming solar radiation reflected or scattered from the surface of the earth, while active remote sensing uses artificially-generated energy sources, such as radar, to receive information reflected back from objects. Understanding the interactions of light energy with the atmosphere and the water column is essential to retrieving bathymetry from satellite-deployed, passive optical sensors such as the QuickBird imager. The following is a summary of the principles governing these interactions.

A. PRINCIPLES OF RADIATIVE TRANSFER

Optical remote sensing uses the visible, near-infrared (NIR), and shortwave infrared (SWIR) portions of the electromagnetic spectrum to observe the radiation that is emitted or reflected from targets on the ground or water column. The reflected energy received by the optical remote sensor is the result of interactions from the air-sea interface, atmospheric absorption and scattering, and the biological constituents in the water column (Morel, 1977). The portion of the electromagnetic spectrum sensed by a spectral imager and the pathways of light from the sun to the ocean and back to the sensor are relevant topics to bathymetric studies from remotely sensed data and are addressed below.

1. Electromagnetic Spectrum

The electromagnetic spectrum is classified into several spectral regions. Optical remote sensors typically exploit the visible portion of the electromagnetic spectrum when conducting bathymetric studies from space based sensors: its ability to penetrate water makes it the most favorable for extracting water depth information. The visible portion of the electromagnetic spectrum extends from about 400nm (blue-violet light) to 700nm (red light). Additionally, solar radiation that is reflected in the near-infrared band (above 700nm) from surfaces above sea water is often used when analyzing multispectral images

of coastal environments (Robinson, 2004). Although the water column in the near infrared wavelengths absorbs most of the solar radiation before it returns to the sensor, this band is typically exploited in the preprocessing portion of image analysis (Robinson, 2004). Figure 1 depicts the portions of the electromagnetic commonly used for bathymetric studies.

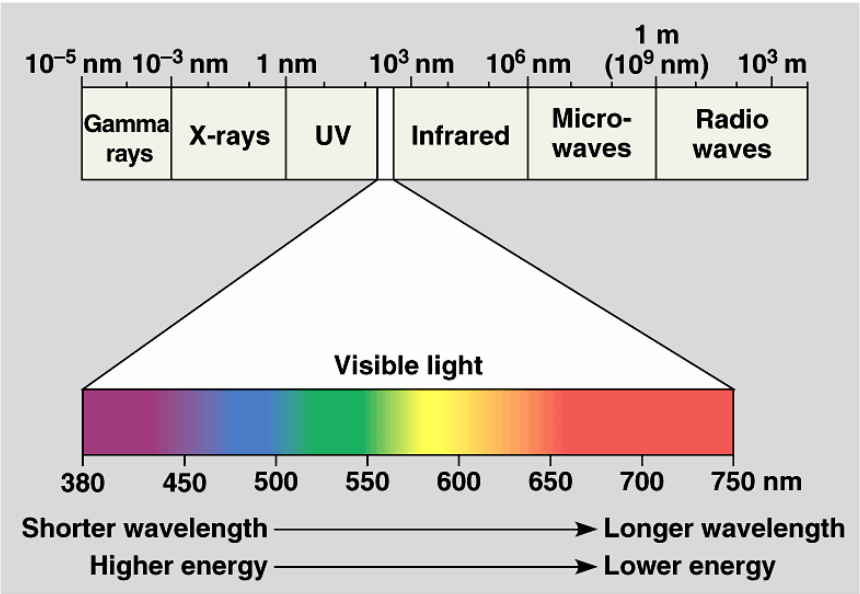

Figure 1. Visible portions of the electromagnetic spectrum (From University of Arkansas at Little Rock 2006).

2. Transmittance, Absorption, and Reflection

The basic interactions of light with matter involve absorption, reflection, scattering, or transmittance (Martin, 2004). The particular type of interaction will depend on the wavelength of incident light, the frequency, and the angle of incidence (Olsen, 2006). Figure 2 illustrates these interactions.

Radiation emitted from the sun must traverse the atmosphere twice before being collected back by a sensor orbiting in space. This translates in solar radiation being absorbed, scattered, and reflected two-fold before reaching the sensor. As will be detailed later in Chapter V, these interactions must be accounted for through a series of image analyses. Furthermore, these interactions are compounded when attempting to retrieve data from benthic environments, due to the influence of the water column.

Reflection of energy from the earth's surfaces is the specific interaction that allows information to be collected by a spectral imager from land or marine targets.

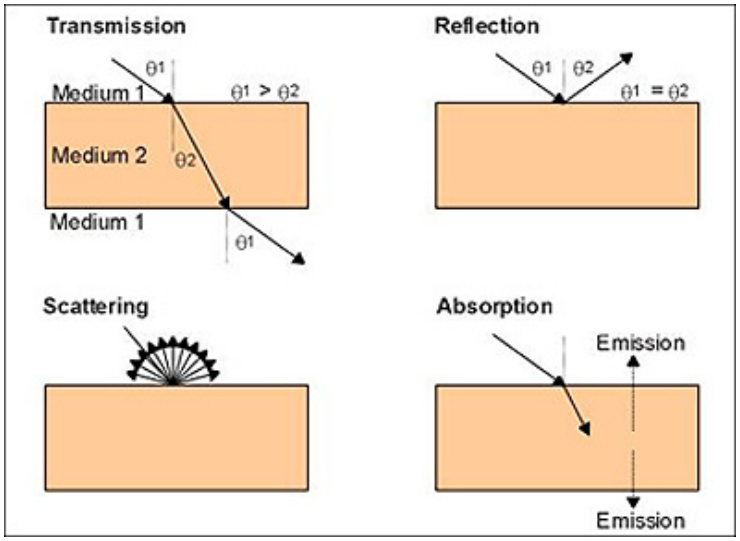

Figure 2. Possible interactions of light matter (From Avery and Berlin, 1992).

3. Spectral Signatures

Spectral signatures are the variations in reflected or absorbed electromagnetic radiation at varying wavelengths, which may identify particular objects. For any given material, the amount of reflectance, absorption, or scattering will depend on wavelength (Olsen, 2006). The relationship between the energy that is reflected, absorbed, or transmitted is used to determine the spectral signature of an object on the ground or in the water. Spectral signatures make it possible to either positively identify certain substrates (Short, 2006), as in the case of certain minerals using hyperspectral imagery (Lillisand and Kiefer, 2004), or distinguish them from other substrates as in the case of vegetation types illustrated in Figure 3. Each substrate type has spectral characteristics that can be used to distinguish it from other objects. Substrates in marine benthic environments (e.g. coral reefs) can also be characterized by their spectral signatures (Lubin et al., 2001). Sand for example, has a much higher reflectance at visible wavelengths than do other objects, such as coral or algae. Figure 4 illustrates some common coral reef benthic substrates.

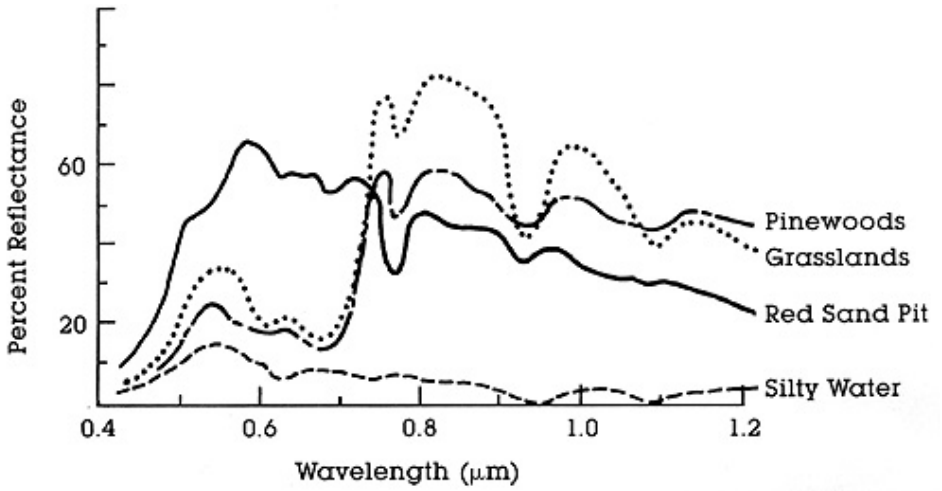

Figure 3. Spectral signatures of common terrestrial objects (From Short, 2006).

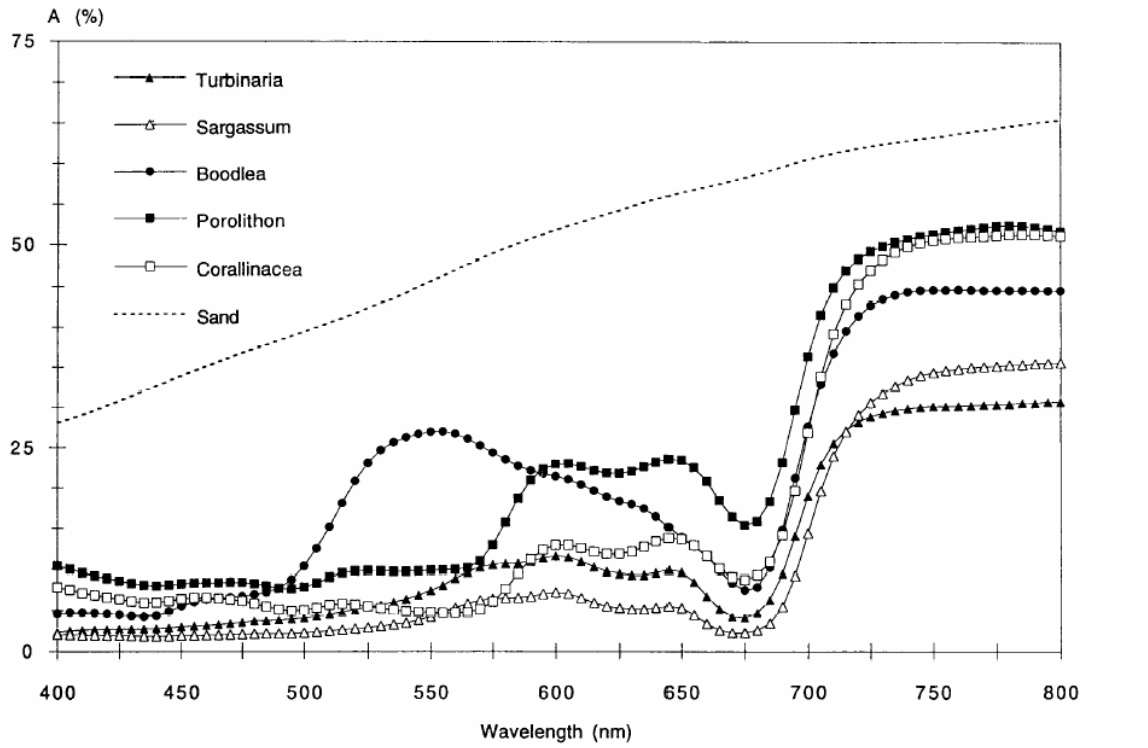

Figure 4. Albedo values for different forms of algae and coral (From Maritorena et al., 1994).

B. INTERACTIONS OF LIGHT WITH THE ATMOSPHERE

Electromagnetic radiation traveling through the atmosphere undergoes several changes based on its wavelength. Primary effects are absorption and scattering.

1. Atmospheric Absorption

The atmosphere absorbs incoming energy primarily due to water, carbon dioxide, and ozone (Lillesand and Kiefer, 2004). Atmospheric absorption is highly dependant on wavelength. The atmosphere will absorb most of the energy transmitted at wavelengths below 350nm and above 10 microns. At these wavelengths, the atmosphere is considered opaque: most of the energy is not transmitted. However in the visible and near infrared portions of the spectrum, most of the incoming energy is transmitted through the atmosphere. This is commonly referred to as a spectral window (Thomas and Stamnes, 1999) and is illustrated in Figure 5. Since the majority of energy is transmitted through the atmosphere in the visible/near infrared bands, optical remote sensors often exploit these regions of the spectrum.

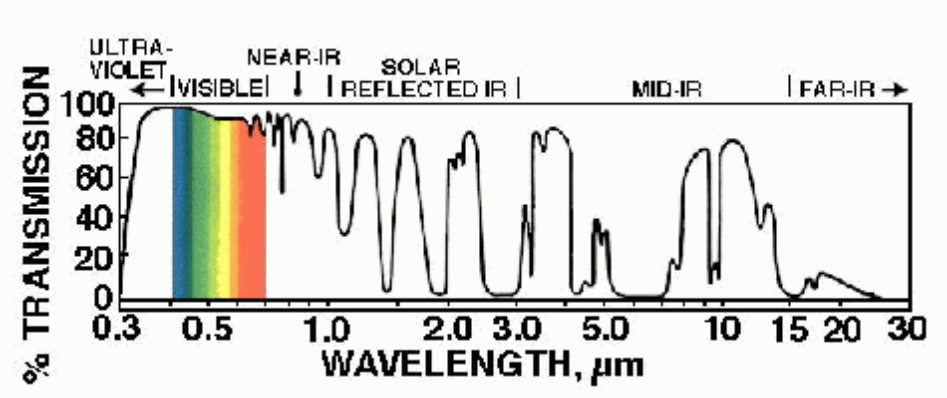

Figure 5. Absorption spectrum (From http://rst.gsfc.nasa.gov/Into/Part2_3.html).

2. Atmospheric Scattering

Atmospheric scattering results from the interaction of radiation with gas molecules and aerosols (suspended particles). Such is the magnitude of this interaction that in a oceanic image, only 8 – 10 percent of the signal corresponds to oceanic reflectance, the rest due to scattering (Mishra et al., 2005). There are two primary consequences of atmospheric scattering: 1) radiant energy is reduced, and 2) there is unwanted gain at the sensor (Martin, 2004). Scattering can be subdivided in Rayleigh and Mie scattering. Rayleigh scattering is the scattering of energy by particles that are smaller than the wavelength of energy. Since Rayleigh scattering is inversely

proportional to the fourth power of wavelength, shorter wavelengths are scattered more than longer wavelengths (Lillisand and Kiefer, 2004). This type of scattering is most noticeable in the visible wavelengths. Mie scattering occurs when the diameter of atmospheric particles is similar to the wavelength of the energy being radiated. Common examples of Mie scattering are smoke, dust, and water vapor. Atmospheric gases and particles are also responsible for radiance that is scattered and reaches the sensor without contacting the earth's surface. This is referred to as path radiance (Green et al., 2000). Path radiance is therefore also defined as the radiance recorded at the senor resulting solely from the downwelling solar and sky radiation (Jenson, 2000).

3. Atmospheric Correction for Spectral Imagery

The effects of the atmosphere on incoming radiation can be expressed mathematically. Figure 6 details the primary interactions of energy within the atmosphere as it radiates the ocean surface and returns to the sensor. Mishra (2005) divides the radiance $L_t(\lambda_i)$ received by the sensor at a particular wavelength λ_i into several components:

$$L_t(\lambda_i) = L_r(\lambda_i) + L_a(\lambda_i) + T(\lambda_i) L_g(\lambda_i) + t(\lambda_i) L_w(\lambda_i) \quad (1)$$

where $L_r(\lambda_i)$ and $L_a(\lambda_i)$ are radiances gathered in the atmosphere by scattering, T is direct transmittance, $L_g(\lambda_i)$ is the contribution from specular reflectance of sunlight from the sea surface, t is the diffuse atmospheric transmittance of the atmosphere, and $L_w(\lambda_i)$ is the water leaving radiance. The last component contains the data that is needed to derive bathymetric data. Once the atmospheric effects can be corrected for, the equation is simplified, and bathymetric retrieval is dependent solely on light interactions with the water column.

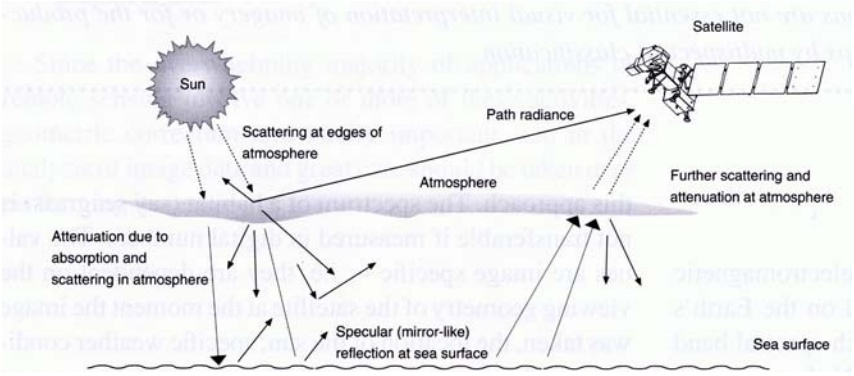

Figure 6. Interactions of energy with the atmosphere (After Green et al., 2000).

C. INTERACTIONS OF LIGHT AND WATER

Optical processes in the water column must be accounted for to successfully derive information about benthic environments from remotely sensed data, and they are considered more complex than atmospheric interactions due to the variety of interactions that take place (Robinson, 2004). Since light is readily absorbed by water, optical remote sensing is usually confined to shallow clear waters, where light can penetrate up to 30 or 40m. Sea water contains an abundance of dissolved and particulate matter. These particles are optically important and their concentration varies in the water column both spatially and temporally (Mobley, 1994). The optical properties of the water column have been traditionally divided into two distinctive classes: the inherent and apparent optical properties (Smith and Baker, 1981).

1. Inherent Optical Properties (IOPs)

Inherent optical properties are those properties that depend only upon the medium and are independent of the ambient light field within the medium (Mobley, 1994). When sunlight enters the water column, it will interact with the particles in the water. These particles will cause the incident light to be altered by scattering or absorption (Thomas and Stamnes, 1999). The scattering and absorption characteristics are defined as inherent optical properties of water (IOPs). The two fundamental IOPs are the absorption and scattering coefficient. These can be specified by the spectral absorption coefficient, spectral scattering coefficient, and spectral beam attenuation coefficient (Mobley, 1994).

The spectral beam coefficient can be used to determine the light loss due to absorption by dissolved and particulate matter as well as scattering in pure water by

particulates (Mobley, 1994). Figure 7 illustrates the dependence on wavelength for the absorption and scattering coefficients. Absorption increases below 400nm and above 600nm wavelength range. Moreover, the scattering coefficient is at its minimum at visible wavelengths and increases rapidly in the lower wavelengths. The graph demonstrates how visible wavelengths are ideal to carry out remote sensing in oceanic environments.

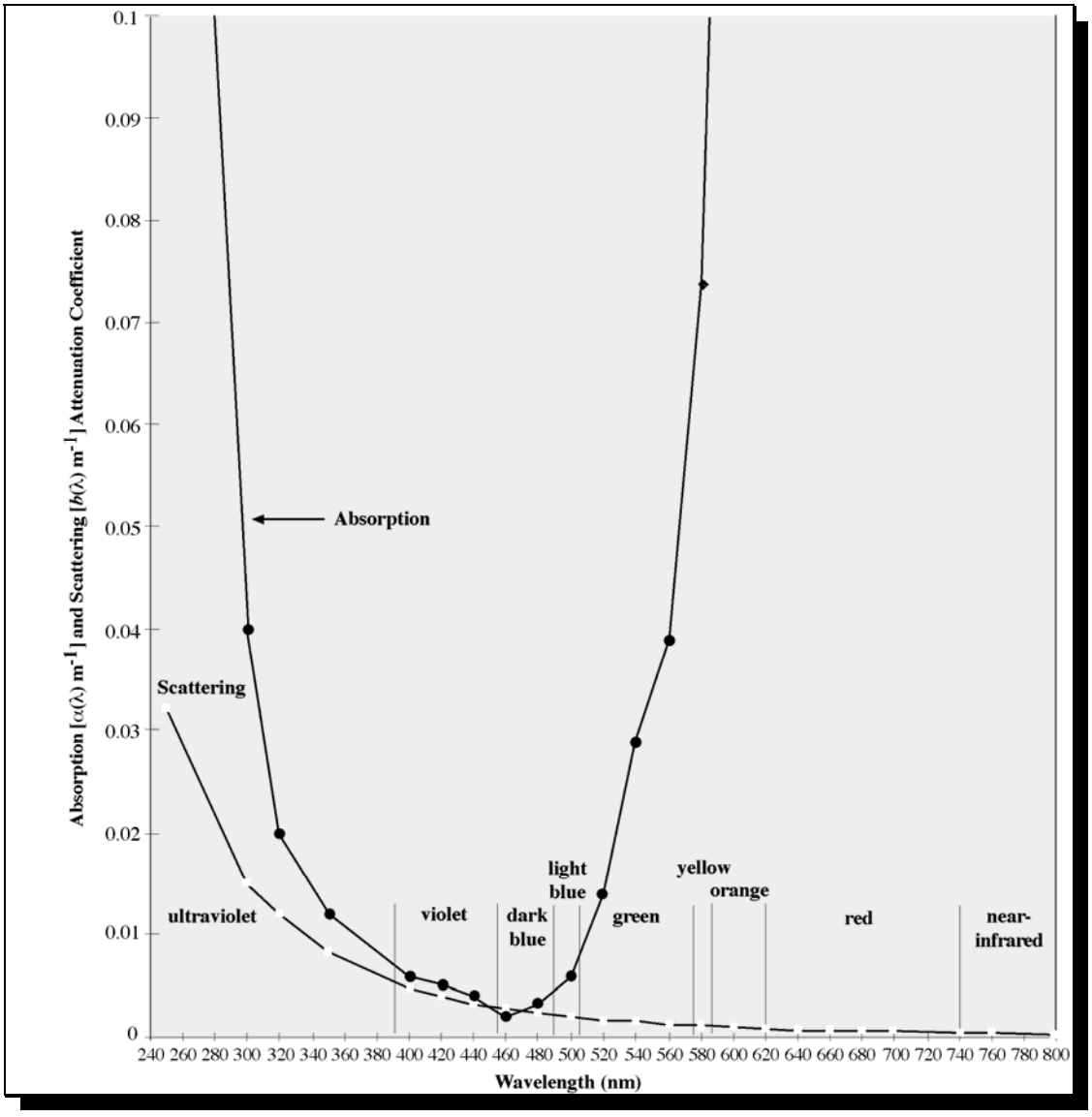

Figure 7. Water absorption and scattering (From University of California Santa Barbara Department of Geography 2006).

2. Apparent Optical Properties (AOPs)

An optical property is apparent if it is dependent on the medium and on the directional structure of the ambient light field (Mobley, 1994). Much like inherent optical properties, apparent optical properties (AOPs) are also dependent on the dissolved particles and sediment in the water column. Unlike IOPs, these properties cannot be measured *in situ* since they depend on the ambient radiance (Mobley, 1994). The following AOPs are most relevant to bathymetric studies for retrieving estimates of the water parameter concentrations: average cosines, reflectance, and diffuse attenuation coefficients (Mobley, 1994; Robinson, 2004).

The average cosine, u, is a useful characterization of the angular distribution of the light field in the water body at given point. This can be regarded as the average cosines of photons in the water column at a particular point shown by

$$\mu(z;\lambda) = \frac{E_d(z;\lambda) - E_u(z;\lambda)}{E_o(z;\lambda)} \tag{2}$$

where the values of E_d, E_o and E_o are the downward, upward, and scalar irradiances (Mobley, 2004).

The spectral irradiance reflectance $R(z;\lambda)$ is defined as the ratio of spectral upwelling to downwelling plan irradiances (Mobley, 2004). The downwelling irradiance, E_d is measured just above the surface and the upwelling irradiance, E_u is measured just below the surface:

$$R(z;\lambda) = \frac{E_u(z;\lambda)}{E_d(z;\lambda)} \tag{3}$$

This parameter is often evaluated immediately below the water surface at depth z at a particular wavelength.

The spectral remote sensing reflectance, R_{rs}, is defined as the ratio of water leaving radiance L_w, to the downwelling irradiance, E_d (Doxaran, 2006). This relationship can be calculated just above the water's surface:

$$R_{rs}(\theta,\phi;\lambda)=\frac{L_w(\theta,\phi;\lambda)}{E_d(\theta,\phi;\lambda)} \tag{4}$$

The remote sensing reflectance is important in that it calculates the amount of downwelling light incident on the water's surface that is returned though the surface in a particular direction to the collecting sensor.

Light is attenuated exponentially with depth due to absorption and scattering properties of the water column. This decrease in intensity of light as a function of depth is expressed mathematically by Beer's law as:

$$E(z)=E(0)e^{(-Kz)} \tag{5}$$

$E(z)$ and $E(0)$ are the irradiances at a given depth and the surface. K is the attenuation coefficient and z is depth. Beer's law can then be modified to take into account changing sun illumination and downwelling irradiance at several depths:

$$E_d(z;\lambda)=E_d(0;\lambda)e^{-\int_0^z K_d(z';\lambda)dz'} \tag{6}$$

One of the most important optical properties of sea water is the diffuse attenuation coefficient, $K_d(z,\lambda)(m^{-1})$. This AOP provides a direct measure of penetration of radiant energy in the water column and is expressed as:

$$K_d=(z;\lambda)=-\frac{1}{E_d(z;\lambda)}\frac{dE_d(z;\lambda)}{dz} \tag{7}$$

Although this coefficient is classified as an apparent optical property, it is principally determined by the IOPs in the water column and not so much to the ambient light field (Kirk, 1994; Mishra, 2005).

Finally, it is important to mention that Jerlov (1976) developed a classification scheme of oceanic waters based on the spectral profile of K_d, and that this scheme is still widely used today in the optical oceanography community. According to Jerlov, Type I waters are extremely clear waters: Type II waters have greater attenuation and greater amounts of organic constituents in the water column: Type III waters are more turbid and

have much less clarity. Coral reef environments like Midway Atoll generally fall between Type I and Type II waters since they are generally very clear and light penetrates farther than in other coastal waters. For this reason, coral reef environments are particularly ameneable to optical remote sensing studies.

Figure 8 illustrates the basic interaction of lights as it propagates through the water column.

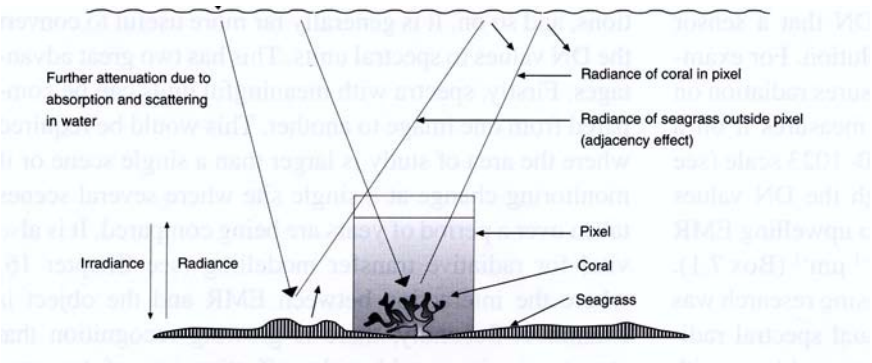

Figure 8. Interaction of energy with the water column (After Green et al., 2000).

D. OPTICALLY SIGNIFICANT CONSTITUENTS OF NATURAL WATERS

The composition of the water column directly influences the level of absorption and scattering of photons. As mentioned, absorption and scattering properties in the water column itself will considerably modify the spectral reflectance of an object at depth (Lyzenga, 1981). In addition, the abundant organic and inorganic compounds in the water will increase the attenuation in the visible wavelengths. The primary substances in ocean waters that significantly alter the light entering the water column are dissolved substances and particulate matter.

1. Dissolved Matter

Ocean water contains numerous dissolved substances. The substances increase scattering in the ocean and have limited effects on the absorption of light in the visible wavelengths. The predominant dissolved substance in the ocean is salt. The ocean average salinity is about 35 parts per million and significantly increases scattering of incoming irradiance (Mobley, 1994).

Colored dissolved organic material (CDOM) or yellow matter is associated with decayed phytoplankton and consists mostly of humic and fulvic acids (Robinson, 2004).

These compounds are highly absorbent within ultra violet-blue wavelengths and decrease at the longer wavelengths, and are most dominant in coastal waters where runoff can flow into rivers and lakes. In remote ocean locations, CDOM plays a much smaller role and other constituents, such as particulate matter, may be more prevalent.

2. Particulate Matter

Particulate matter in the oceans is a major contributor to absorption. Organic particulate matter is primarily represented by phytoplankton, whose highest absorption is in the blue and red wavelengths. The amount of chlorophyll *a*, a dominant photosynthetic pigment, will proportionally increase the amount of light absorption in a body of water.

Inorganic particles enter the water as dust, soil, or river runoff into coastal areas. When suspended sediment is present in the water column, much of the reflected energy returned to the sensor is from the sediment and not from the benthic environment (McCoy, 2005). In shallow oceanic environments, suspended sediments are often present due to wave and wind action.

E. ALGORITHMS FOR BATHYMETRY DERIVATION FROM SPECTRAL IMAGERY

For depth to be retrieved using spectral imagery, the light reflected from the surface of the ocean, the contributions from the water column, and the atmospheric effects all have to be removed (Zhongping et al., 1999). There are several radiative transfer equations that are used to derive water depth from remotely sensed data. Numerous methods for deriving bathymetric data are based on several implicit assumptions and range in complexity (Lyzenga, 1978, 1981; Benny and Dawson, 1983; Philpot, 1989). Some algorithms calculate bottom reflectance assuming that water properties are homogeneous and light is attenuated exponentially with depth (Lyzenga, 1978, 1981; Philpot, 1989). These are referred to as “linear methods”. Other radiative transfer equations that have been developed (Stumpf et al., 2003) are based on the ratio of two or more bands (“ratio method”).

1. Linear Method

There are two primary assumptions made by linear methods discussed in this section: i) light is attenuated exponentially with depth in the water column. ii) water

quality is consistent within the particular image (the attenuation coefficient, K, remains constant) (Louchard, 2003; Green et al., 2000). Several of the variables in this section have been modified for consistency.

a. Lyzenga (1978, 1985) Method

Lyzenga (1978) derived a linear relationship to determine water depth applying the two assumptions mentioned above. Lyzenga (1985) developed a technique that could use one or more wavelengths depending on the water column. If the optical properties of the water and the bottom reflectance are uniform, a single wavelength band can be used to describe the relationship between water depth and radiance. The fundamental principle for this technique is derived from Beer's law (eq. 8). The relationship between the radiance to depth and bottom reflectance can be expressed as:

$$R_{rs} = \left(A_b - R_\infty\right) e^{(-gz)} + R_\infty \tag{8}$$

where A_b is the irradiance reflectance of the bottom (albedo), R_∞ is the reflectance of the water column, and g is a function of the diffuse attenuation coefficient for upwelling and downwelling light. This equation can be solved for depth and expressed as:

$$z = \frac{1}{g}\left[\ln\left(A_b - R_\infty\right) - \ln\left(R_{rs} - R_\infty\right)\right] \tag{9}$$

Lyzenga (1985) further developed a technique to determine water depth if the optical properties are not uniform. In this case, two or more bands are applied to the equation (above) and a linear solution is derived:

$$Z = a_o + a_i X_i + a_j X_j \tag{10}$$

where $a_{o,} a_{i,} a_j$ are derived constants for the waters optical properties and X is the transformed radiance at a particular band. This method provides a solution for bottom albedo and does not assume the reflective properties of bottom substrates are constant throughout the scene. Since the intensity of light is assumed to be decaying exponentially with depth, radiance can be linearised using natural logarithms. If X_i is the transformed radiance, the equation can be written as:

$$X_i = \ln[R_w(\lambda_i) - R_\infty(\lambda_i)] \tag{11}$$

This method is difficult to implement due to the complexity of having to solve for five variables. Furthermore, to derive accurate depth from this method, the substrates must be identified and depth indices for each substrate have to be calibrated individually (Hedley, 2005).

b. Benny and Dawson (1983) Method

Benny and Dawson (1983) provide another method of predicting bathymetry. This method makes the additional assumption that the reflective properties (or albedo) remain constant throughout the scene. This method assumes the light received at the sensor follows a certain path through the water column. Depth can be determined through an algorithm that takes into account the light path from the sea surface to the bottom and back up to the sea surface (Green et al., 2000). Additionally, specular reflection from the sea surface and atmospheric scattering are taken into account. This method is given by:

$$z(depth) = \frac{\log_e\left(L_x - L_d\right) - \log_e\left(L_o - L_d\right)}{-k\left(1 + \cos ec\left(E^{'}\right)\right)} \tag{12}$$

where L_x is the signal receive at the sensor from water depth x, L_d is the signal received by the senor from deep water, L_o is the signal receive by the sensor for shallow water, and $E^{'}$ is the sun elevation angle that is corrected for the water column. The light path to calculate the sun angle elevation is described in detail in Figure 9.

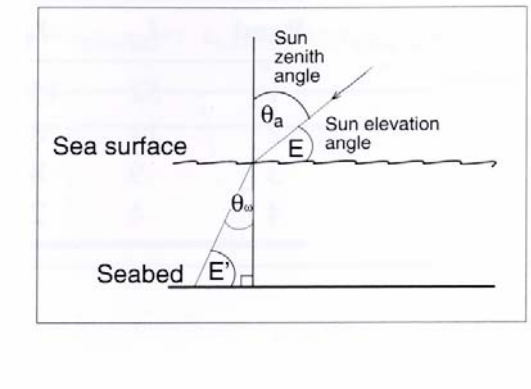

Figure 9. Radiation path in the water column to determine sun angle elevation (From Green et al., 2000).

c. Jupp (1988) Method

Jupps' method makes the same assumptions as Benny and Dawson (1983). This method is composed of three parts to determine water depth. These are: (1) the calculations of depth of penetration zones (DOP) (2) the interpolation of depths within penetration zones (3) and the calibration of depths within the zones (Green et al., 2000). This method is based on the fundamental principle that radiation is attenuated at different rates as it penetrates the water column. Different wavelengths will be attenuated until they becomes extinct at a certain depth. The maximum depth that each band can penetrate will be recorded as a depth penetration zone for that band. Each DOP will essentially be assigned a maximum floor. Furthermore, each DOP must be calibrated in order to obtain the most realistic values for the algorithm. This is usually performed over a homogenous substrate, such as sand. After these steps are performed, the depth can be calculated with the expression:

$$z(depth) = \sum_{i=1}^{N} \frac{\ln\left(L_e\right)_i}{-2k_i N} - \sum_{i=1}^{N} \frac{\ln\left(L_b\right)_i}{-2k_i N} \tag{13}$$

where L_e is the measured radiance at the sensor, N is the number of spectral bands, and L_b is the radiance at the seabed or albedo. Figure 10 depicts the DOPs for Landsat Thematic Mappper bands 1-4. As shown, the maximum penetrating depths for each bands is indicated by $z_1 - z_4$. The blue band has the maximum depth of penetration while the NIR has the lowest. These values are used to identify the boundaries for each DOP zone.

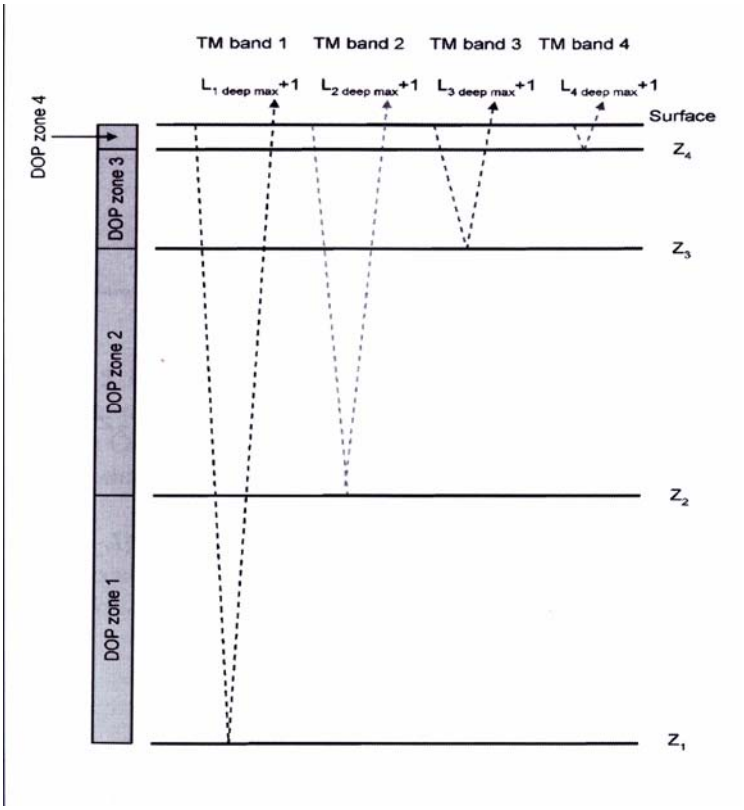

Figure 10. Depth of Penetration Zones (DOP) for Landsat bands 1-4 (From Green et al., 2000).

d. Philpot (1989) Method

Philpot (1989) developed an expression to derive depth that incorporated the effects of the water column and atmospheric properties. This expression includes factors such as the air-sea interface, atmospheric effects, and illumination. This is expressed by:

$$L_d(z) = CE_d(0-)\left(A_b - \rho_\infty\right)^{-gz} + CE_d(0-)\rho_\infty + L_{sg} + L_{path} \tag{14}$$

L_d is the radiance received at the sensor over water depth z, C is a transmission factor for the atmosphere and water surface, $E_d(0-)$ is the downwelling irradiance just below the water surface, R_∞ is the irradiance reflectance of optically deep water, and L_{sg} is the sun glint. Melsheimer and Liew (2001) express this equation after the measured radiance is converted to apparent reflectance R. If apparent reflectance for

deep water, as well as the surface and attenuation coefficients are known, depth can be retrieved through the expression:

$$z = -\frac{1}{g}\left(\log\left[R(z) - R(\infty)\right] - \log\left[R(0) - R(\infty)\right]\right) \quad (15)$$

The apparent reflectance can be determined with high resolution multispectral images, but the attenuation coefficients must be determined through other means (Mobley, 1994).

2. Ratio Method

The accuracy of the above methods of predicting water depth varies due to the variation in bottom albedo and the reflective properties of bottom substrates (Green et al., 2000). Much of the errors are due to failure of the algorithms to discern between different albedos. Furthermore, dense substrates, such as sea grass may be confused with deep water. The lack of ability to map bottom features with lower reflectance than adjacent deep waters was the initial motivation for Stumpf et al. (2003) to develop a new technique.

This ratio method is based on absorption rates of different wavelengths. Different bands will be attenuated at different rates as energy penetrates the water column. As depth increases, the band with a higher absorption rate will decrease proportionally faster than the band will a lower absorption rate. Consequently, the ratio between the two bands will increase as depth increases. This concept effectively removes the error associated with varying albedo since both bands are affected in the same way. Accordingly, the change in the ratio between the bands will affect the higher absorption band more with increasing depth: therefore, as depth increases, the change in ratio between the two bands will be affected more by depth than by bottom albedo. With these premises, varying bottom reflectances at the same depth will have the same change in ratio. Depth can then be approximated independently from bottom albedo with:

$$z = m_1 \frac{\ln\left(nR_w\left(\lambda_i\right)\right)}{\ln\left(nR_w\left(\lambda_j\right)\right)} - m_0 \quad (16)$$

where m_1 is a tunable constant to scale the ratio depth, n is affixed constant for all areas to assure that the algorithm is positive under all circumstances, and m_o is the offset for a depth of 0m.

In contrast to the linear method, the ratio method contains only two tunable parameters and can be applied quickly and effectively over large areas with clear water. This method claims to be more robust and applicable in waters with different bottom substrates.

III. PREVIOUS WORK AT THE NAVAL POSTGRADUATE SCHOOL

Bathymetric studies have been extensively pursued by the Navy. Stuffle's (1996) thesis used hyperspectral imagery to derive shallow water depth estimates over a small region of Lake Tahoe, California. This was accomplished by identifying different substrates and estimating the reflectance values for each substrate type. Depth was then determined for each region separately using their respective values of bottom reflectance. The results demonstrated that it was possible to derive depth from remotely sensed hyperspectral data. As a follow-on, Fisher (1999) assessed the applicability of the method used by Stuffle (1996) using a different hyperspectral sensor and covering a much larger area of Lake Tahoe. Additionally, the author had *a priori* knowledge of one bottom type and was able to use this known bottom reflectance in a computer algorithm to derive depth. The results obtained by Fisher (1999) determined that improved accuracy can be obtained with limited *a prior* knowledge of bottom type. In particular, this thesis follows previous work by Clark (2005) and Densham (2005).

A. CLARK (2005)'S STUDY

Clark (2005) compares several different methods to derive water depths. The author used the Veridian Multi-Spectral Toolkit (VMST) software and Stumpf et al. (2003)'s ratio method to obtain depth measurements. This was performed using high resolution data acquired from the QuickBird and IKONOS satellite sensors. Each method was applied to two multi-spectral images provided by the two satellite sensors at Looe Key, Florida. The results were then compared to data obtained from a LiDAR survey.

The tests were conducted over the clear waters of Looe Key which consisted of highly variable depth and bottom substrates. Several transects were selected because of variability in substrates and depth. The criteria for each transect was to select locations that had variable depth but homogenous substrate, variable substrate but homogenous depth, and variable depth and variable substrate.

The results demonstrated that the ratio method proved sensitive to bottom type. It produced shallower depths over bottom types with low albedo and deeper depths over bottom types with high albedo. This is in contrast to Stumpf's claim that this method is

independent of bottom substrate. Another trend noted by the author was that sun glint has some affect on the overall results. Furthermore, the ratio method failed completely in this study at depth less than 1 meter over sand and coral. Finally, the maximum depth obtainable using the ratio method was 15 meters. This was caused by the absorption of the green band at depth.

As demonstrated in Clark's thesis, the ratio method is affected by variable bottom types. This method was altered by the varying reflectances of sea grass, coral, and sand. Clark 2005 concluded that both algorithms used in his paper would benefit from more consideration for bottom substrate in the scene. The incorrect outputs of depth for different substrates indicate that this technique could be potentially improved through pre-classification of bottom substrate.

B. DENSHAM (2005) STUDY

This thesis focused on two methods in which to derive water depth, the ratio method and the Stratified Genetic Algorithm. The objective was to compare the performance of these methods when calculating depth in different water conditions and clarity. This was performed using high resolution data acquired from the QuickBird satellite sensor. The test areas selected were based on the water clarity and turbidity of the water column. The areas chosen were the clear waters of Looe Key, FL and the turbid waters Plymouth Sound, UK. Atmospheric correction was performed using the NPS Aerosol Model and over-water dark object approach. Sea surface correction was conducted using Hochberg et al. (2003) method to remove glint from the image. Water column corrections were performed using the HYDROLIGHT program to determine the attenuation coefficient, k_d. Additionally, HYDROLIGHT requires a value for the amount of chlorophyll in the water column, so a chlorophyll analysis was conducted to input into the program. Once these parameters were corrected, they were inputted into the depth deriving algorithms and the results were compared.

The results obtained by Densham (2005) determined that variable bottom types, light attenuation, surface waves, and non-homogenous water influenced each method.

Specifically, variable bottom types affected the ratio method significantly. This was primarily caused by misinterpretation of dark finger coral with deep water when performing the ratio method.

Densham (2005) also recommended that variable bottom type should be analyzed individually for a potential improvement to depth outputs.

The logical next step from these results is to test the hypothesis that the ratio method is sensitive to bottom type. This hypothesis will be tested by producing a classification of the benthic habitats, and use it to subset the imagery into different substrates. The ratio method of bathymetry derivation will be applied to the whole image and again to the subsetted images representing different substrates, and compared the accuracy of the depth retrieval against nautical chart depths.

THIS PAGE INTENTIONALLY LEFT BLANK

IV. TEST SITE

A. NORTHWESTERN HAWAIIAN ISLANDS MARINE NATIONAL MONUMENT

The Northwestern Hawaiian Islands Marine National Monument (NWHI) is the largest marine conservation area in the world and consists of dozens of islands, atolls, reefs and shoals (Figure 11). This designation was established by Presidential Executive Order as recently as June 15, 2006, and replaced an earlier designation as Coral Reef Ecosystem Reserve established in 2000. The NHWI archipelago is located northwest of the main Hawaiian Islands with its southeastern extreme approximately 120 nautical miles from the island of Kauai and its northwestern most point at Kure Atoll (28.4N, 178.5 W). The NWHI National Monument extends more than 2,000 km in length and is over 180 km wide. The area covers more than 13,000 square kilometers of coral reefs and is home to thousands of land and marine species. The archipelago is mostly uninhabited and is surrounded by some of the most extensive coral reefs in the world (Eilperin 2006). Unlike the main Hawaiian Islands and most of the world's remaining coral reefs, the archipelago boasts some of the healthiest and least disturbed coral reef ecosystems on earth. Notably, the NWHI represents nearly 70 percent of all coral reefs located in U.S. waters (Siciliano, 2005). Its clear waters, diverse substrates, and abundance of healthy coral make it an ideal environment to perform bathymetric studies.

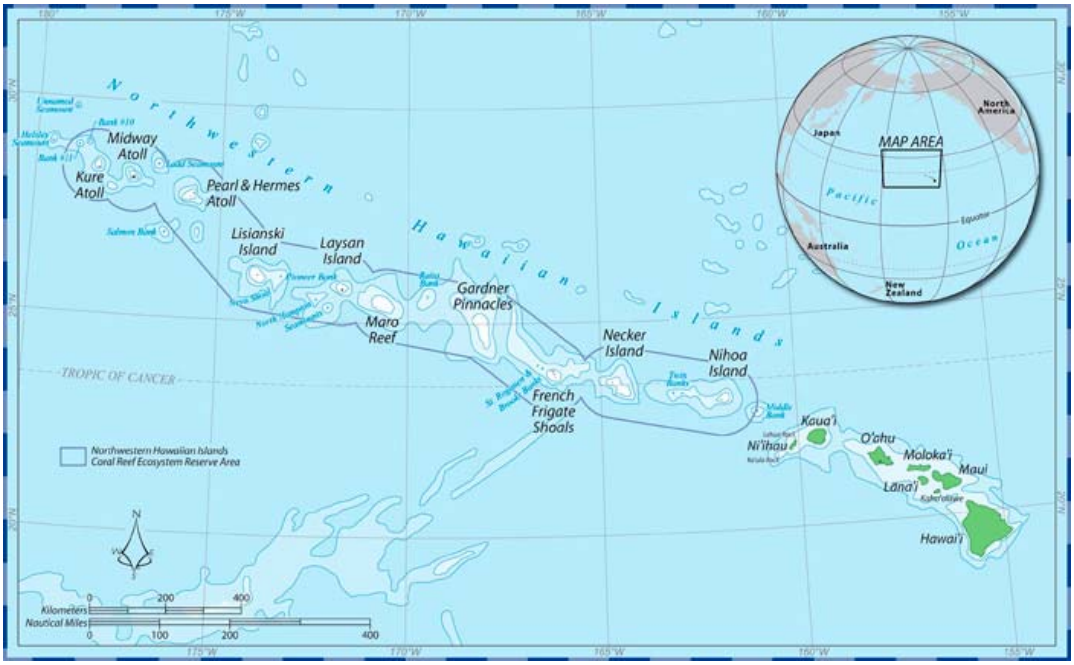

Figure 11. Northwestern Hawaiian Island Marine National Monument (From http://www.hawaiireef.noaa.gov).

B. MIDWAY ATOLL

Midway Atoll is the most recognizable of all the NWHI due to the strategic importance of the island during WWII. Midway Atoll is located at approximately 28°N and 177°W and about 2,300 km west-northwest of Honolulu. Midway Atoll consists of over 1500 acres of land and its nearly circular rim is approximately 6 miles in diameter (Morris, 2005). The atoll consists of the three main Islands of Sand, Eastern, and Spit. Sand Island is the largest of the three islands and measures 1.8 miles by 1.2 miles wide or about 1200 land acres (Morris, 2005). Eastern Island is located approximately 1 mile east of Sand Island and occupies approximately 334 acres (Morris, 2005). Spit Island is a small unvegetated islet and covers only about 6 land acres. An encircling submerged rim protects the lagoon waters of Midway Atoll. The depth of the atoll ranges significantly from emerging reefs to a maximum depth of approximately 25m near the center of the lagoon. Outside the atoll, the depth ranges from 3m in the near fore reef and quickly increases to about 30m just seaward from the atoll's rim in a dramatic drop-off typical of oceanic atolls. Figure 12 shows the locations of the main islands and coral rim. There are currently 51 reported species of stony coral found in the atoll along with sea grass,

urchins, sponges, sand channels, and algae (Maragos et al., 2004) There are two large benthic categories found inside the reef at Midway Atoll: (1) areas of bare sand and rubble, and (2) reef habitats of coral and algae species.

Midway Atoll was home to the United States Navy and has fairly reliable navigational charts and soundings. The United States Navy altered the atoll significantly during WWII to accommodate seaplanes and a functional harbor. The lagoon was dredged and the southern portion of the atoll was cleared to create a passage into the lagoon. The navigational charts were revised in 2000 and provide fairly accurate depths inside the atoll.

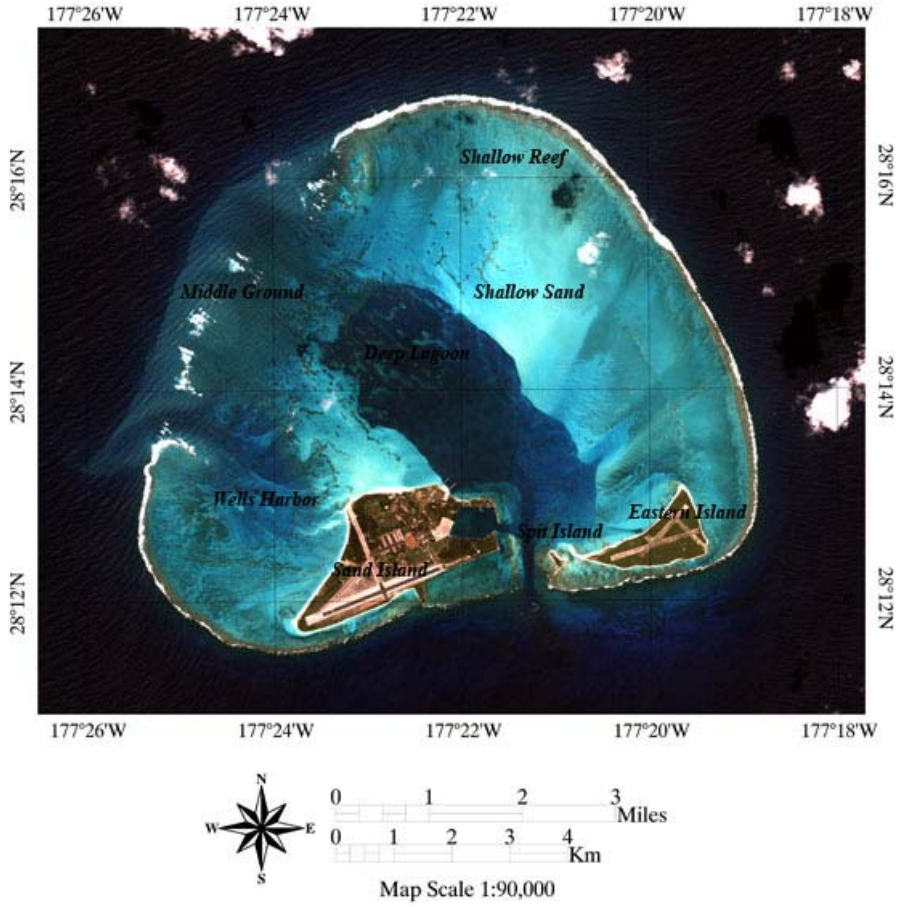

Figure 12. The 2004 QuickBird image of Midway Atoll used in this study, with annotated habitats.

THIS PAGE INTENTIONALLY LEFT BLANK

V. MATERIALS AND METHODS

A high resolution multispectral image of Midway Atoll was acquired by the QuickBird satellite on October 12, 2004 at 22:34:29 GMT.

A. MATERIALS

1. QuickBird Satellite Sensor

A product of DigitalGlobe, Inc., the QuickBird satellite system (Figure 13) was launched in 2001 and is currently the highest resolution sensor available commercially, boasting a panchromatic band with a 60cm spatial resolution and a multispectral system with a 2.4m resolution. The sensor acquires data in four spectral bands covering the blue, green, red, and near-infrared wavelengths, plus a panchromatic band. The swath width of the sensor is 16.5km at nadir, or a strip at 16km by 165km. The nominal ground sample distance (GSD) at nadir is .61m panchromatic and 2.44m for multispectral imaging. The sensor is also capable of a 30 degree off nadir viewing angle, which ultimately affects the GSD. Table 1 provides a summary of the characteristics of the QuickBird satellite system.

Launch Date	18-Oct-01
Orbit Altitude	450 Km
Orbit Inclination	97.2º, sun-synchronous
Equator Crossing Time	10:30 a.m. (descending node)
Orbit Time	93.5 minutes
Revisit Time	1-3.5 days depending on Latitude (30º off-nadir)
Swath Width	16.5 Km x 16.5 Km at nadir
Metric Accuracy	23-meter horizontal (CE90%)
Digitization	11 bits
Resolution	Pan: 61 cm (nadir) to 72 cm (25º off-nadir)
	MS: 2.44 m (nadir) to 2.88 m (25º off-nadir)
Image Bands	Pan: 450 - 900 nm
	Blue: 450 - 520 nm
	Green: 520 - 600 nm
	Red: 630 - 690 nm
	Near IR 760 - 900 nm

Table 1. QuickBird data (From DigitalGlobe, 2004)

Figure 13. QuickBird Satellite (From Prasert, 2005).

2. Software

a. Environment for Visualizing Images 4.2 (ENVI)

Environment for Visualizing Images 4.2 was used as the computational utility to analyze the image of Midway Atoll for this research. ENVI 4.2 is an image processing system designed for multispectral and hyperspectral data analysis and information extraction. ENVI 4.2 is written in the Interactive Data Language (IDL), which is a programming language that provides integrated image processing and display capabilities (Research Systems, 2004). ENVI 4.2 was used to process the QuickBird imagery for application of the radiometric conversion algorithms, sea surface correction, masking of features, water column correction technique, and benthic image classifications. Furthermore, ENVI 4.2 was used to apply the ratio method to retrieve bathymetry and extract depth profiles.

b. ATCOR 8.7

ATCOR 8.7 is a software add-on package to the digital imagery-processing package ERDAS IMAGINE. Produced by Leica Geosystems Geospatial Imaging, ATCOR 8.7 removes the effects of scattering and absorption caused by the earth's atmosphere. ATCOR 8.7 contains two variants for processing: ATCOR2 for flat terrain (2 dimensional) and ATCOR 3 (3 dimensional) for rough terrain. ATCOR 2 was used in this thesis for atmospheric correction because of the low relief that characterizes coral atolls. The program has several functionalities, such as haze removal, atmospheric correction, and the capability of viewing reference spectra of selected targets (Leica

Geosystems, 2006). Although this program has the ability to perform haze removal for an image, this function was not used in this research due to the algorithm's inability to remove haze over water.

B. METHODS

An important part of image analysis is the pre-processing involving radiometric radiance conversion of the image from digital numbers to spectral radiance, atmospheric correction, glint removal, and correction for the water column. Once these process have been complete, classifications for the image can be performed with subsequent application of the ratio method for bathymetry derivation.

1. Spatial Subsetting

A spatial subset was performed on the original image of Midway Atoll to remove portions of the image that are unnecessary for analysis, and reduce processing time. The subset aimed at removing the deep water pixels on the outer regions of the image and a large number of cloud pixels and cloud shadows also in the outer regions of the image.

2. Radiance Conversion

The QuickBird satellite sensor records the intensity of electromagnetic radiation as digital numbers (DN). The range of values of digital numbers depends on the particular sensor and the environmental conditions, so these values are arbitrary (DigitalGlobe, 2003). The radiometric corrected pixels are specific to the QuickBird sensor and must be converted into radiance (L) to perform spectral analysis or comparison to other images (DigitalGlobe, 2003). The calibration information provided by DigitalGlobe in the image metadata file (found in appendix A) was used to convert DN to top-of-atmosphere spectral radiance. As specified by Digital Globe (DigitalGlobe technical file, Radiometric use of QuickBird data, 2005), the process for converting images depend on both the bit depth and the generation time of the image. To convert to spectral radiance, the radiometrically corrected image pixels are multiplied by the absolute radiometric calibration factor, K. This step is defined in equation 17.

$$L_{Pixel,Band} = absCalFactor_{Band} * q_{Pixel,Band} \tag{17}$$

The band-specific, absolute radiometric calibration factor, K, is located in the image metadata file. The results are then divided by the effective bandwidth to obtain

spectral radiance in units of $W/m^2/sr/\mu m$. The QuickBird effective bandwidths used are shown in Table 2. The equation used is:

$$L_{\lambda_{Pixel,Band}} = \frac{L_{Pixel,Band}\left(W - m^{-2} - sr^{-1}\right)}{\Delta\lambda_{band}\left(\mu m\right)} \tag{18}$$

The QuickBird calibration utility employs the image metadata file to convert the relative radiance into absolute radiance. This step was performed using a preprocessing utility in ENVI 4.2.

Spectral Band	Effective Bandwidth [μm]
Pan	0.398
Blue	0.068
Green	0.099
Red	0.071
NIR	0.114

Table 2. QuickBird Effective Bandwidths ($\Delta\lambda$) (From DigitalGlobe, 2003).

3. Atmospheric Correction

The atmospheric correction of high-resolution images is an important step to improve data analysis. ATCOR 8.7 was initially used to radiometrically and atmospherically correct the image. The utility provided by ATCOR 8.7 resulted in overcorrected values for the image. The program appeared to be overcorrecting the image in the red wavelengths, which produced erroneous negative values for many pixels in the red band. Negative values in measured spectra are an indicator that one or more of the set parameters are not adequate (Leica Geosystems, 2006). Additionally, the reflectance profiles in the corrected image were compared to the typical reflectance values found in Table 3 and were found not to be in the typical value ranges. In an attempt to obtain reliable values, multiple iterations were performed by changing the set parameters in the program. A range of aerosol concentration (or visibility) was adjusted to improve the reflectance values in the corrected image. The value for visibility was initially set to 20km and adjusted accordingly to obtain improved image outputs. The ATCOR atmospheric correction function also depends on the sensor view angle. This value was calculated using the technique described in the calibration manual for

IKONOS (Leica Geosystems, 2006). Another modifiable parameter in the program is the model for the solar region. This selection takes into account the aerosol and atmosphere type. A sample spectral profile of vegetation before and after atmospheric correction is shown in Figure 14. Although the image produced many negative values in the red band, the corrected image was tested further to perform more analysis before being abandoned. The corrected image produced by ATCOR 8.7 was used to perform the sea surface correction, water column correction, and classification. However, the overcorrection error was compounded with each step: the sea surface correction output produced negative reflectance values in the red band over water. This error was amplified when attempting to correct for the water column. As a result of the overcorrected values produced by the atmospheric correction algorithm in ATCOR 8.7, this step was removed in the analysis process.

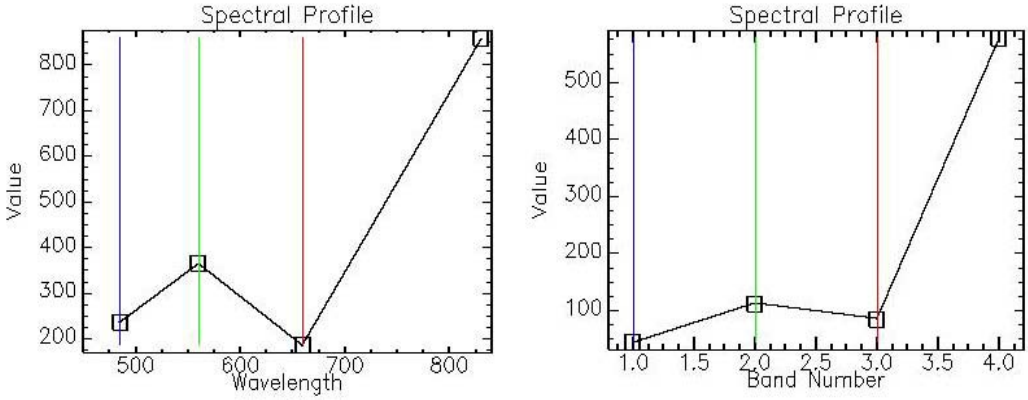

Figure 14. Spectral profiles for vegetation before and after performing atmospheric correction with ATCOR 8.7.

Target	Blue (0.49µm)	Green (0.55µm)	Red (0.66µm)	NIR (0.84µm)
water	3 - 5	4 – 6	2 - 3	0 - 1
dense dark veg.	0.5 - 2.5	2 – 5	1 - 3	16 - 25
green vegetat.	3 - 6	6 – 12	4 - 8	35 - 50
agricultural soil	4 - 8	7 – 12	10 - 15	15 - 25
asphalt (dark)	8 - 9	9 – 10	9 - 10	10 - 12
asphalt (bright)	14 - 16	16 – 18	16 - 19	18 - 22

Table 3. Typical reflectance values (%) in different parts of the spectrum (From Leica Geosystems, 2006).

4. Conversion to Top-of-Atmosphere Spectral Reflectance

This step was performed due to our inability to use ATCOR 8.7 to output a functional corrected image. The process outlined by DigitalGlobe (2005) was followed to convert the image from radiance to apparent reflectance. The image is converted to apparent reflectance by correcting for Earth-sun distance, solar zenith angle, and the image acquisition Julian Day. This information was extracted from the image metadata file. Additionally, the solar geometry for the image was determined. This is important since variations in the spectral irradiance are subject to the solar geometry for a particular image (DigitalGlobe, 2005). The method used to obtain the top-of-atmosphere band-averaged reflectance is given:

$$\rho_{\lambda_{Pixel,Band}} = \frac{L_{\lambda_{Pixel,Band}} * {d_{ES}}^2 * \pi}{Esun_{\lambda_{Band}} * \cos(\theta_s)} \tag{19}$$

The band averaged solar spectral radiance, $E_{SUN_{\lambda Band}}$, are in units of $W - m^{-2} - \mu m^{-1}$ and had to be converted to the proper units before implementation in ENVI 4.2. The Earth-sun distance, d_{ES}, uses the Julian Day acquisition time. The solar zenith angle is found by subtracting the sun elevation angle at the time of image acquisition (found in the image metadata file) from 90 degrees. The values are then incorporated into the Band Math expression in ENVI 4.2 to obtain the converted image.

5. Glint Removal: Hochberg et al. (2003) Method

A common problem associated with high resolution imagery over water is the specular reflection of sunlight on ocean surfaces, due to wind generated waves. This problem was addressed with a technique first described by Hochberg et al. (2003) and then by Hedley et al. (2005) to remove sunglint from remotely sensed imagery. This method exploits the maximum absorption and minimal water leaving radiance of the NIR band, which was used to characterize the spatial distribution of relative glint intensity. The image was then scaled to absolute glint intensities which were subtracted from the visible bands, resulting in glint intensities that were reduced or eliminated in the outputted image. The two working assumptions are (1) that water exhibits very strong absorption of NIR wavelengths (this is warranted by observing very low water leaving radiance values at NIR wavelengths, including at shallow depths where NIR water-

leaving radiance is minimal regardless of bottom type - Hedley, 2005); (2) that the real index of refraction in the visible bands is nearly equal to the NIR band. From these premises, a linear relationship exists between the NIR and visible bands given that the amount of light that is reflected from the water column in the NIR band is a good indicator of the amount of light reflected in the visible bands (Hochberg et al., 2003).

In Hochberg et al. (2003), two independent pixels, the brightest and darkest, were used to establish a linear relationship between the visible and NIR bands. Hedley et al. (2005) on the other hand pointed out that a larger area of interest should be selected over optically deep water to obtain a linear relationship between the NIR and visible bands. This modification was used to select areas of interest over optically deep water in the QuickBird image of Midway Atoll.

The step was performed after image subsetting and conversion to Apparent Reflectance. As pointed out by the authors, this method also performs a first order atmospheric correction. A sample area (Region of Interest, or ROI) was selected over optically deep water for the NIR band. Several ROIs were selected around the atoll in areas exhibiting a range of sun glint, where the optically deep water appeared homogenous. Pixels from these regions were used to regress the NIR band against each visible band. Figure 15 shows an example output for the NIR band regressed against the red band. The slope of this regression was obtained using the expression: $b_1 - (.897 * b_2)$. In this case, b_1 is the red band and b_2 is the NIR band. Subsequently, all land and cloud features were masked using the NIR band values by thresholding the image to high reflectance values, since the water pixels are characterized by low reflectance while emergent features, such as land and cloud, exhibit higher returns. This process masked most emergent features even though some manual fine tuning was necessary to remove any remaining emergent pixels. The image is then redisplayed in true color with the effects of sun glint removed or reduced, as shown in Figure 16 and 17.

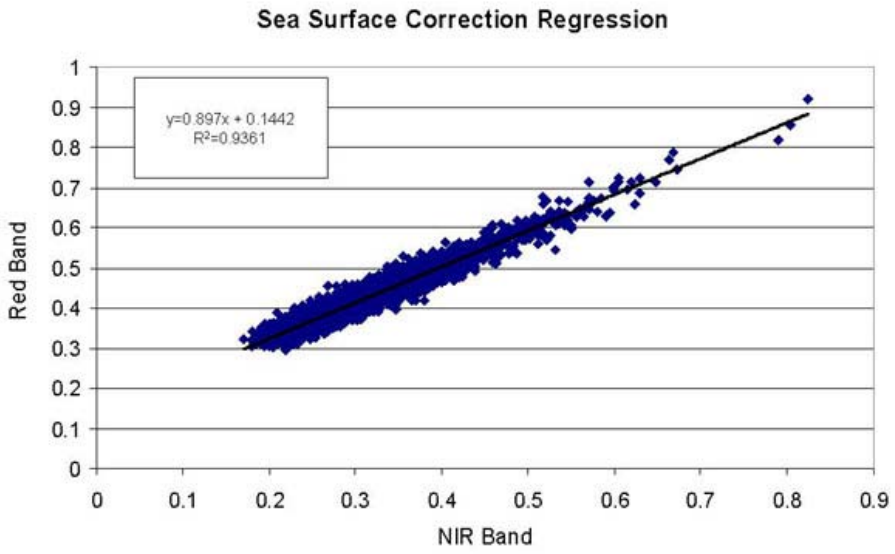

Figure 15. Bi-plot of the NIR band and Red band for sea surface correction.

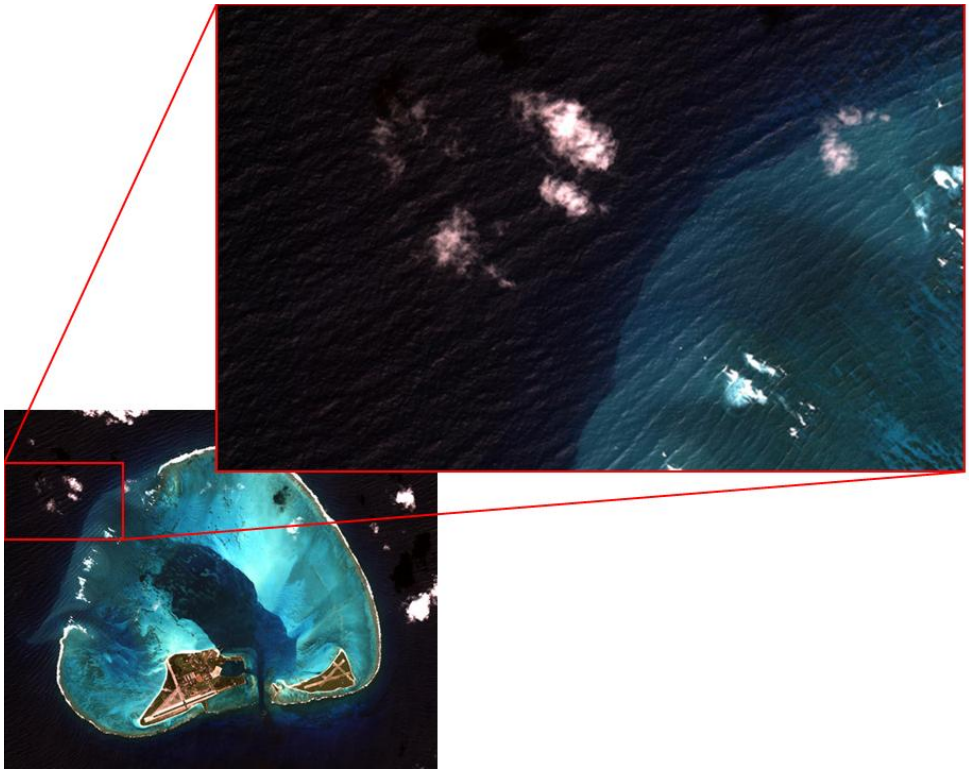

Figure 16. QuickBird image of Midway Atoll before sea surface correction was applied.

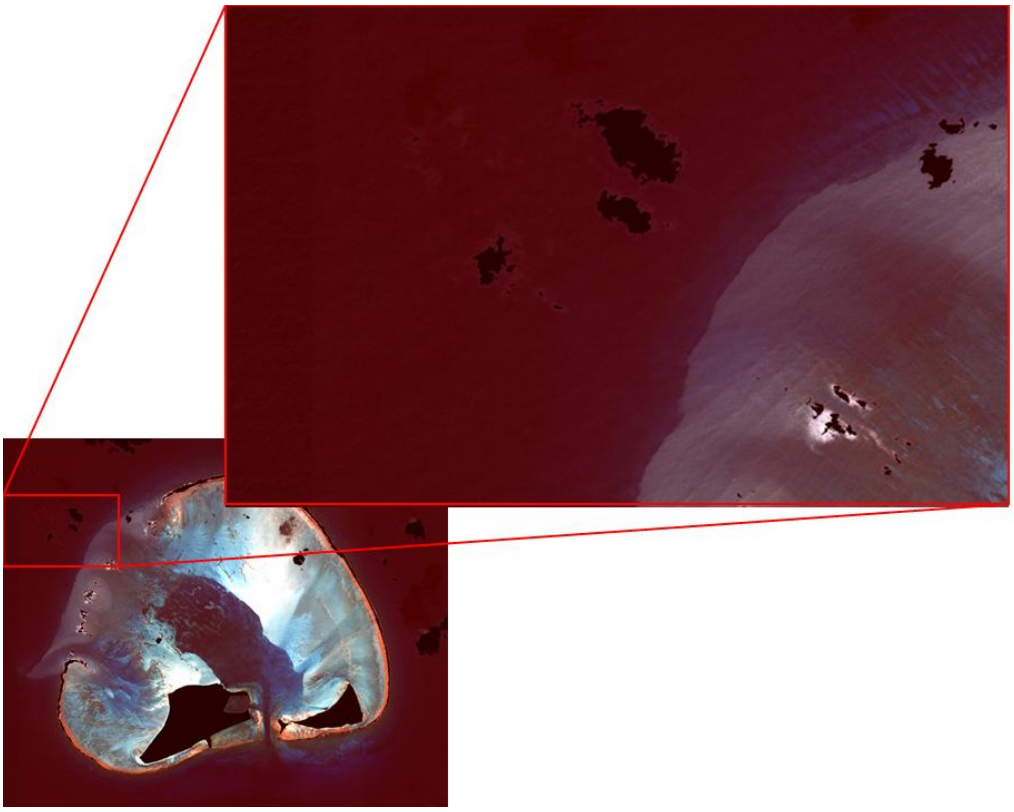

Figure 17. Results of applying Hochberg et al., (2003) sea surface correction algorithm.

6. Water Column Correction: Mumby et al. (1998) Method

An important processing step when measuring underwater environments is to correct for the effects of the water column, to compensate for exponential light intensity decrease with increasing depth. As mentioned in Chapter II (section C and D), this light attenuation is due to absorption and scattering in the water column. Additionally, attenuation is dependent on wavelength, with the red wavelengths attenuating more rapidly than the blue wavelengths. This becomes important when attempting to identify benthic substrates: the spectral signature of sand at 15m, for example, may be similar to coral reflectance at 3m. The classification accuracy of underwater substrates has been shown to significantly increase by compensating for variable depths using this method (Mumby et al., 1998).

The water column correction technique performed here is based on a model by Lyzenga (1978, 1981) and expanded upon by Mumby et al. (1998). This technique

produces a depth invariant band for each pair of visible spectral bands. The visible bands' reflectance values were transformed using natural logarithms, following the steps outlined in Mumby et al. (1998). Six random locations of uniform substrate (sand) over variable depths were selected in the Midway Atoll image, and regions of interests were created. Natural logarithm transform was applied to their pixel values. For atmospherically corrected images, this first step is written as:

$$X_i = \ln(L_i) \tag{20}$$

The transformed radiance of the pixel, X_i, is the natural log of the pixel radiance, L_i in band i.

The next step was to calculate ratios of attenuation coefficients, k, for band pairs. Pairs of spectral bands were chosen, and bi-plots created using the transformed radiances (Figure 18). The slope of the bi-plot is a representation of the attenuation coefficient for those bands. The following equations (from Green et al., 2000) were used to calculate the ratio of attenuation coefficients, where σ_{ii} is the variance of band i, and σ_{ij} is the covariance between bands i and j:

$$\frac{k_i}{k_j} = a + \sqrt{\left(a^2 + 1\right)} \tag{21}$$

where

$$a = \frac{\sigma_{ii} - \sigma_{jj}}{2\sigma_{ij}} \tag{22}$$

and

$$\sigma_{ij} = \overline{X_i X_j} - \left(\overline{X_i} \times \overline{X_j}\right) \tag{23}$$

The bands plotted to calculate the attenuation coefficients were 3 different combinations of the visible bands (green vs. blue, red vs. blue and red vs. green). Before the depth-invariant indexes were processed, the images were masked to exclude land,

clouds, and other emergent features. Three depth invariant bands were created using the given equation:

$$\text{depth-invariant index}_{ij} = \ln\left(L_i\right) - \left[\left(\frac{k_i}{k_j}\right)\ln\left(L_j\right)\right] \tag{24}$$

Each pair of spectral bands produced a single depth-invariant band and these bands were used for classification and interpretation of the image instead of the original reflectance bands (Figure 19).

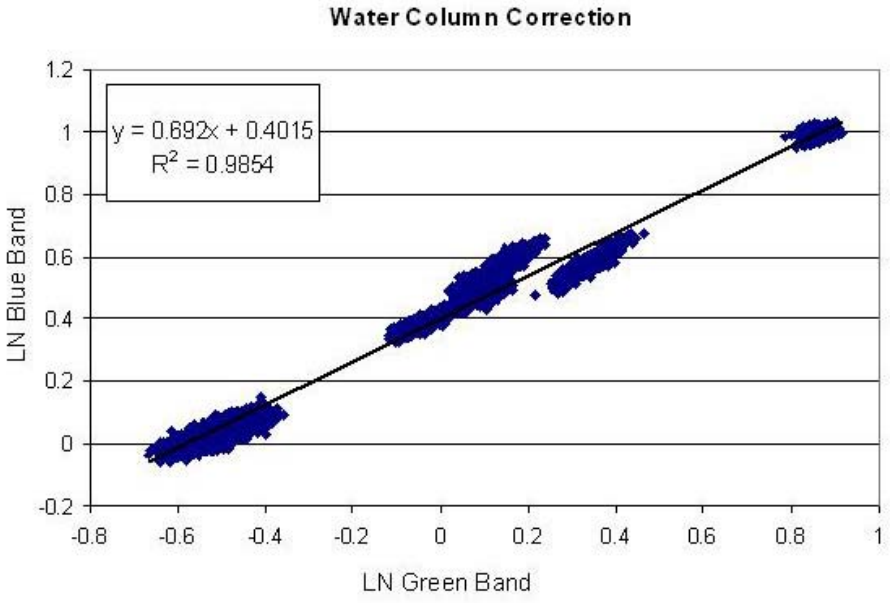

Figure 18. Bi-plot of log transformed pixel values from QuickBird blue and green bands. The pixel clusters represent sand pixels chosen from 5 different depth ranges.

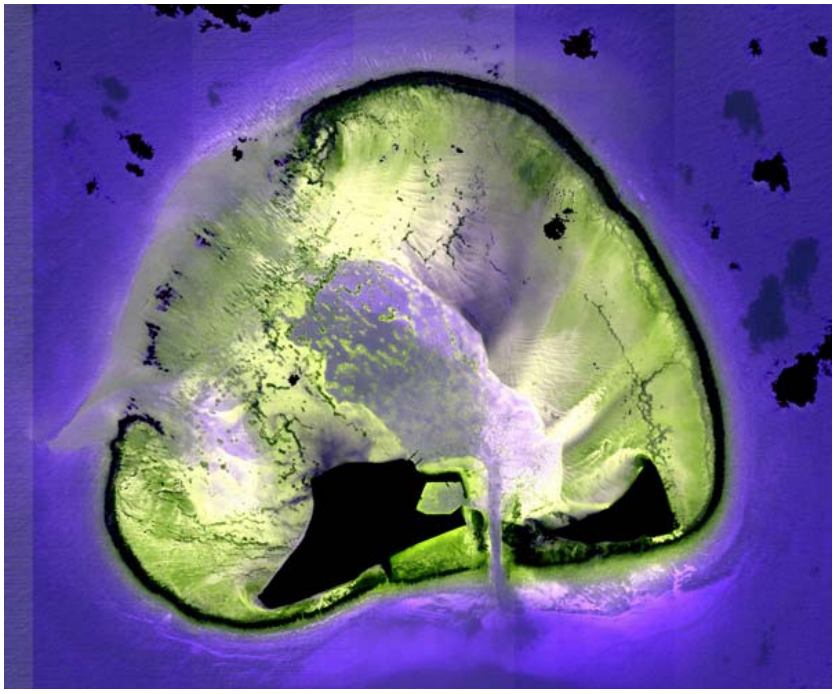

Figure 19. Water column corrected image of Midway Atoll. The black regions are land, cloud, and emerging reef masks.

C. FIELDWORK

To insure a Random Stratified Sampling pattern for the fieldwork, a Iterative Self-Organizing Data Analysis Technique (ISODATA) unsupervised classification was performed on the imagery. Unsupervised classifications use computer generated algorithms to automatically classify pixels into a number of classes based on spectral similarity with no inputs of reference spectra from the user (Green et al., 2000). This method is commonly used as a preliminary guide before conducting any field work. Using the output classes from the ISODATA classification, and the Random Stratified Sampling utility in ENVI 4.2, a total of 80 groundtruth locations over 5 substrates were generated.

Groundtruth field work at these 80 sites at Midway Atoll was conducted over a period of 12 days between June 14-26, 2006. The 2-persons team used an 18-foot Boston Whaler to reach each dive site inside the lagoon (the sites were limited to inside the atoll due to weather and logistical restrictions). The team conducted land and marine surveys with the goals of: 1) collect depth profiles at designated sites, 2) list substrate features for

classification using a hierarchical classification scheme (Appendix B), and 3) collect photographs in order to determine benthic composition.

A total of 80 dive sites were surveyed inside the atoll's marine environment over a 10 day period. The remaining 2 days were utilized to collect data for the other team member's research. Each survey site was located using a GPS handheld (Garmin 60CS). Selection of the dive sites was determined on a day by day basis and was based on weather, boating, and diving conditions. The conditions over the 12-day period were poor due to sustained 20-knot winds, rain squalls, and rough sea state. However, the team was fortunate to have two days of calm, clear weather to conduct boating and dive operations in the shallow back reef environments of the atoll.

Most of the dives were carried out using SCUBA over deeper waters and a combination of SCUBA and snorkel over shallow waters. The team located each dive site and took a GPS reading from the boat. A handheld Sonar System (Hawkeye DF2200PX Portable Sonar System) took an initial depth from the boat over the GPS waypoint. The team then located a safe location for anchorage and gear assembly. A bearing and range was estimated from the anchorage site with the GPS handheld before entering the water. This was sometimes difficult to estimate due to the distance of the anchorage point and the dive site (attempts were made to record GPS points in the water with the handheld unit, but the waterproof container for the GPS handheld failed so this was not possible). The team used the reef habitat classification scheme (Appendix B) to collect information on each dive site within a radius of 10m from the GPS waypoint. At each dive site, another depth was taken from the water surface using the handheld sonar system. The dive team then surveyed the area underwater and collected information for the atoll zone, the geomorphic habitat, bottom cover, and bottom cover abundance. The bottom cover abundance was qualitatively estimated using the scale: D=dominant, A=Abundant, C=Common, O=Occasional, and R=rare. Additionally, a minimum of four photographs were taken of each site, including two panoramic photographs and several close up photographs of the biological and physical substrates.

D. BENTHIC CLASSIFICATION

Categorization of the benthic substrates was performed by analyzing the field data collected at Midway Atoll. A K-means classification was run on the water column corrected image in ENVI 4.2. The desired number of output classes was set to 15-30, the maximum iteration count was set to 50, and the minimum number of pixels in each class was set to 100. The classification process originally yielded 20 different classes throughout the atoll (Figure 20). These were compared to groundtruthed GPS locations. Out of the 20 classes outputted, 8 were identified with the field data. The rest of the classes remained unclassified because they lacked sufficient number of groundtruth points that fell on those classes. The benthic classes defined a diverse range of bottom types, such as live coral, coral/algae mix communities, and turf algae and rubble (Figure 21). Some of these classes were then merged together to be assigned to 1 of 2 benthic categories: 1) different sand substrates and 2) coral/algae communities (Figure 22).

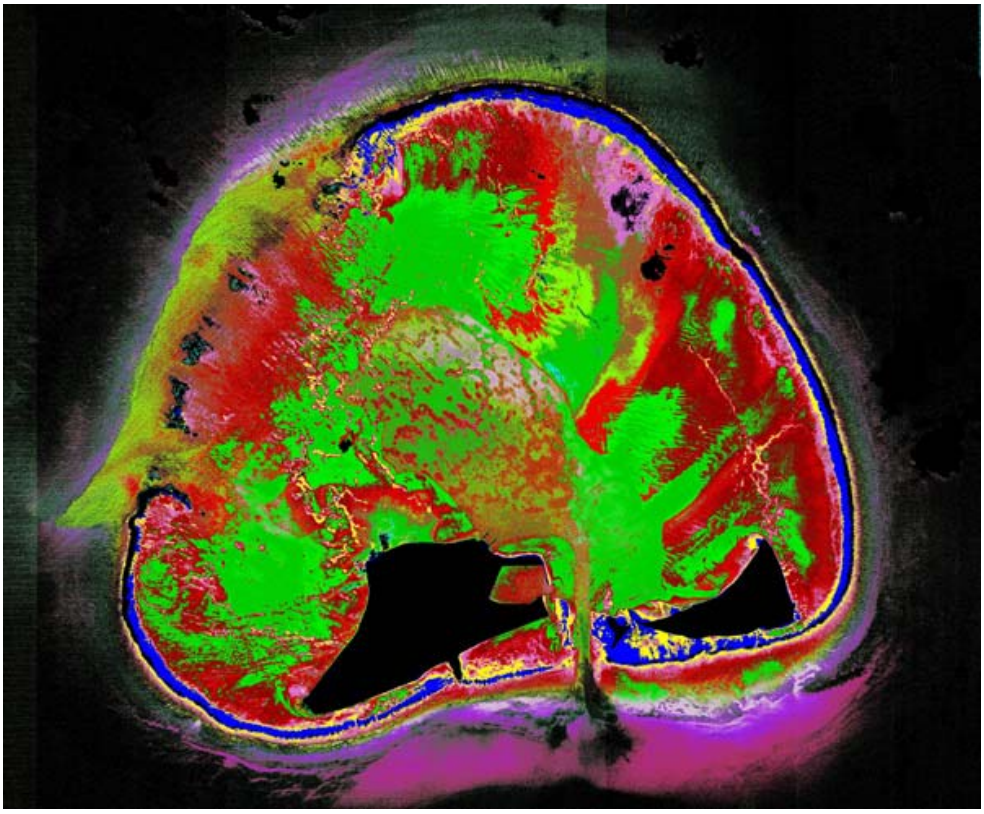

Figure 20. Original K-means classifications yielded 20 classes. Different colors represent different classes.

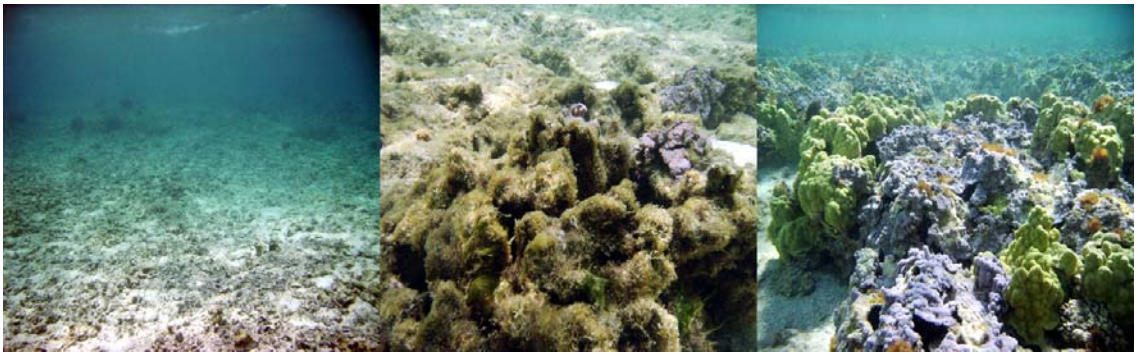

Figure 21. Illustrations representing the different categories used for classification: rubble and sand (left); algae covered coral (center); live coral (right).

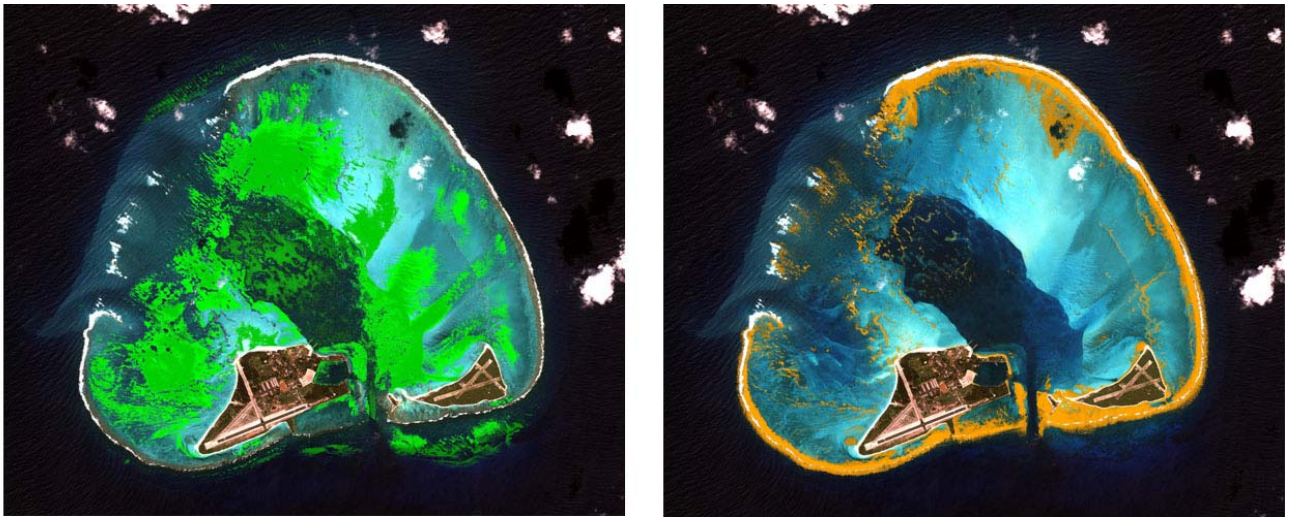

Figure 22. Supervised classifications for sand (left) and coral/algae (right) bottom types. The different variations in color represent different classes in each image.

E. BATHYMETRY DERIVATION

1. Bathymetric Mapping over Entire Image

Bathymetry derivation from spectral imagery is a 2 step process: first relative bathymetry is obtained from the imagery, then absolute bathymetric values are obtained by regressing relative bathymetry values against groundtruthed depth data. The relative bathymetry was calculated using the natural log transformed reflectance values in the blue and green bands on the deglinted reflectance image. The relative bathymetric values for the image were extracted using the expression:

$$\frac{\ln(1000 * b_1)}{\ln(1000 * b_2)} \tag{25}$$

The constant, n, was set to 1000 to assure the algorithm was positive under all circumstances, as suggested by Stumpf et al. (2003). In the expression, b_1 is the blue band and b_2 is the green band. This relative bathymetry was then scaled to absolute depths using depth measurements collected *in situ* at Midway Atoll. To circumvent geospatial errors due to the use of depth values associated to single pixels, a 5x5 low pass kernel convolution was applied to the relative bathymetry values (Siciliano, 2005). Depth values obtained from the surveys at Midway Atoll were regressed against the relative bathymetry convoluted values to find the constant m_1 and m_0 of Stumpf et al. (2003)'s algorithm. These tunable parameters were applied to the ratio algorithm to obtain absolute bathymetry values for the image.

The constants m_1 and m_0 derived from *in situ* depth measurements resulted in the regression being biased toward shallow depths, as can be seen in Figure 23. This problem is attributed to the limited number of deeper depths (>10m) collected inside the atoll, when only 6 points were collected in deep waters (>10m). To obtain a more statistically robust regression, additional points with depth greater than 10m needed to be incorporated into the regression. These additional points with depth values between 10-20m were obtained from the nautical approach chart of Midway Atoll. Care was exercised to insure that soundings from the nautical chart used for tuning were located in areas where the depth values remained relatively constant. Ten additional depth values were used to compliment the groundtruth points collected and used in the regression. The addition of points from the deeper depth range resulted in small statistical improvement of the regression: the R-squared is increased from 0.853 to 0.88 (Figure 24).

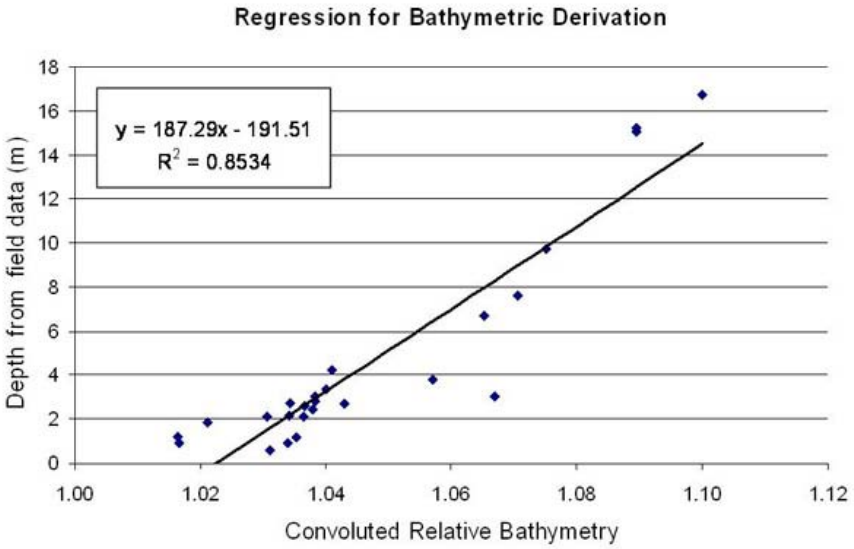

Figure 23. Regression bi-plot for tuning the ratio algorithm using convoluted relative bathymetry and depths from field data and only *in situ* measurements obtained with SCUBA surveys.

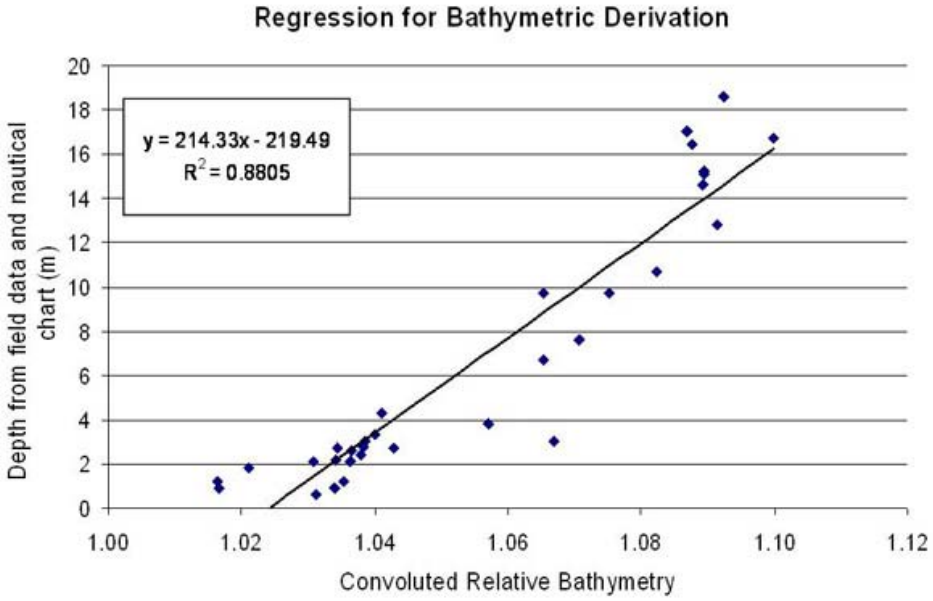

Figure 24. Regression bi-plot for tuning the ratio algorithm using convoluted relative bathymetry and depths measurements from both SCUBA surveys and the nautical chart soundings.

2. Bathymetry over Variable Bottom Types

The benthic classification process and the subsequent merge of similar substrates provided two main benthic classes that defined different sand classes (hereafter referred

to as “sand”), and a mixed coral/algae community (hereafter referred to as “coral/algae”). These two main classes were used to mask and subset the image, resulting in 2 Midway Atoll images representing (1) only the sand substrates, and (2) only the coral/algae substrates. The bathymetry for the two classes was tuned separately using depth values from both the nautical chart and the groundtruth points, following the same process outlined in the previous section for the bathymetry over the entire atoll. A total of 21 points were collected to perform the regression for the coral/algae class and 18 for the sand class. Figure 25 and 26 show the regression outputs for each, which were used to derive the absolute bathymetry for both the image subsets.

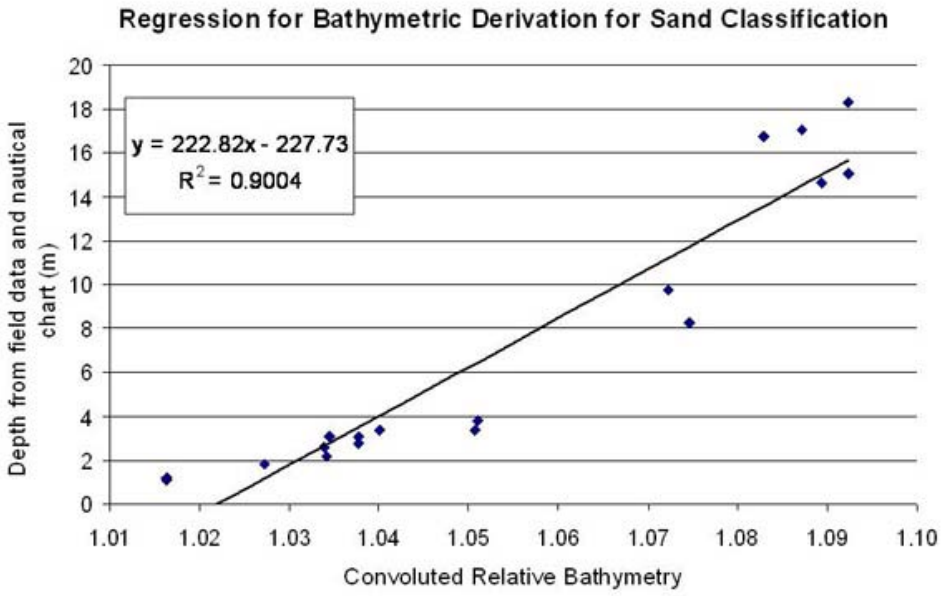

Figure 25. Regression bi-plot for tuning the ratio algorithm over sand substrates.

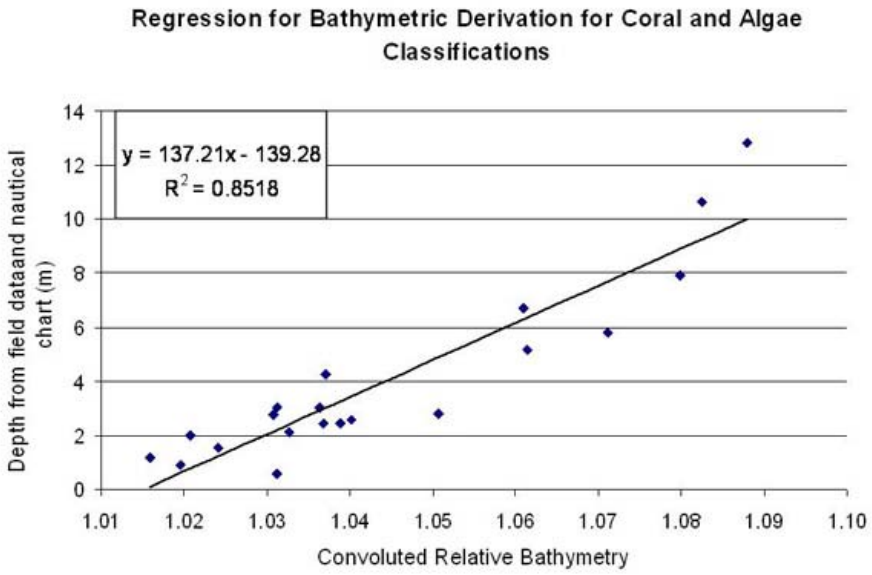

Figure 26. Regression bi-plot for tuning the ratio algorithm over coral/algae substrates.

THIS PAGE INTENTIONALLY LEFT BLANK

VI. RESULTS

A total of three bathymetric maps were generated. These were then assessed using depths obtained from the National Oceanic and Atmospheric Administration (NOAA) nautical approach chart of Midway Atoll. Using the high-resolution satellite image of Midway Atoll, the bathymetry was produced by: (1) applying the ratio method over the entire atoll irrespective of bottom types, and (2) applying the ratio method separately over variable substrates. The accuracy assessment was performed using root mean square (rms) error of the predicted depths compared to the depths obtained from atoll's nautical approach chart.

A. BATHYMETRY FROM ENTIRE IMAGE

Absolute bathymetry was successfully obtained from the QuickBird multispectral imagery for the entire area of Midway Atoll (Figure 27). The major features in the atoll were accurately mapped, such as shallow and deep patch reefs, shallow sand, and coral dominated communities on the back reef. Deeper portions of the lagoon are represented well, such as the deep narrow dredged channel entering the southern portion of the atoll. Figure 27 spans the areas of variable bottom type as well as a large range in depths. Patch reefs located in deeper waters are clearly visible, as well as the sand ripples located in shallow water. The image also clearly details the drastic transition from deep to shallow waters observables in the central lagoon and fore reef environment. The depth retrieved in this bathymetric image ranges from 0 to 22m. This range is in agreement with expected light penetration depths in similar coral reef environments (Stumpf et al., 2003).

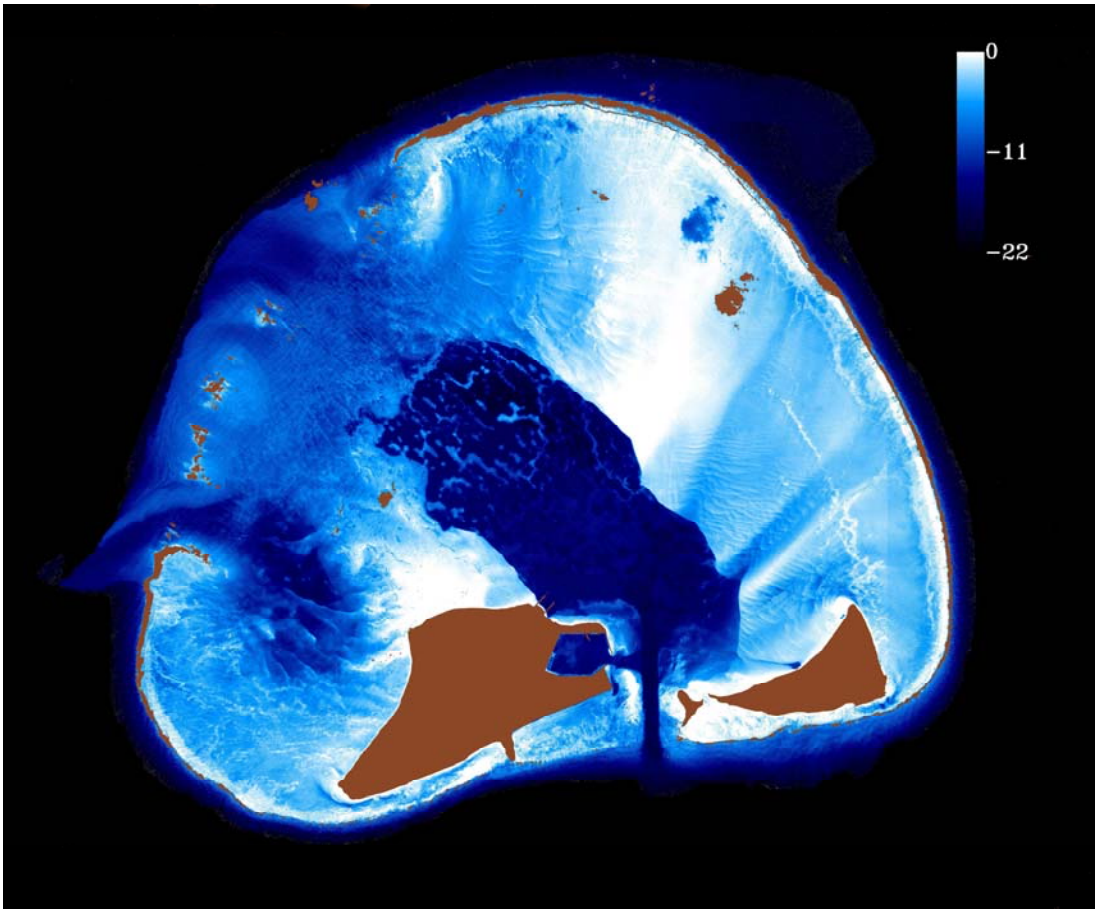

Figure 27. QuickBird derived bathymetry for Midway Atoll using the ratio method. Depths are shown in meters with scale bar at upper right. The brown regions are land, cloud, and emerging reef masks. A mask was also applied to the deep ocean areas seaward of the fore reef.

The algorithm was unable to produce valid depths in very shallow waters, especially over highly reflective surfaces (e.g. sand). In these areas, the algorithm produced negative depth values (i.e. as emergent features above the sea surface). This mostly occurred in areas where the water depth was less than 2m. The results indicate the algorithm failed particularly over surfaces that have high reflectance values. Approximately 10% of the total number of pixels in the image occurs in areas of bright shallow sand or coral, a significant portion of the eastern atoll and on the back reef. The retrieved bathymetry for some of these areas contained negative depths. The majority of the incorrect negative depth values occurred between 0-2.5m. To correct for this, an offset of -2.5m was applied to the image. Figure 28 displays the very shallow regions, where the algorithm ultimately failed to retrieve depth values.

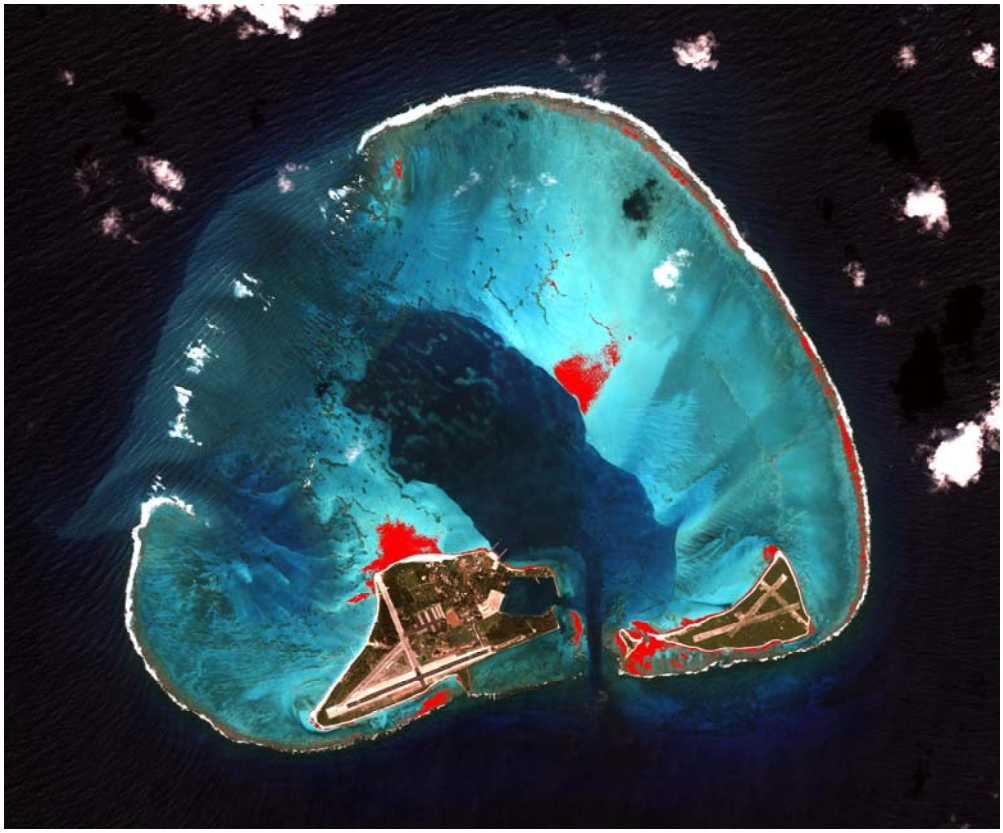

Figure 28. The red regions represent pixels in very shallow water that were excluded due to the high reflectance values and subsequent incorrect depth retrieval.

Furthermore, deeper areas inside the atoll and on the fore reef may be overestimated. When the depth values are compared to the nautical chart, the algorithm produced deeper depth values over dark water pixels in the central lagoon and Wells Harbor than reported in the nautical charts. This error can be attributed to the paucity of points in the deeper depth range collected in the central lagoon and fore reef and used in the regression shown in Figure 23.

B. VARIABLE BOTTOM TYPES

Two separate bathymetric images were produced by tuning the coefficients of the algorithm separately for the two main benthic classes. Applying the ratio method to extract depth separately over variable substrates marginally improved the performance of Stumpf et al. (2003) method. The improvement in resolving bathymetric features is demonstrated in numerous areas throughout the atoll (Figure 29 and 30). Figure 29 shows the shallow coral dominated communities on the back reef and reticulate reef areas. Most noticeably, the depth variations on the back reef are well reproduced, detailing the

transition from deeper to shallower coral. In the deeper waters of the central lagoon, the magnitude of the depth variations are reproduced detailing the transition of low albedo algae-covered coral patch reefs to adjacent sandy bottoms. Sand waves are clearly visible throughout the atoll in Figure 30, despite the variations in depth. Moreover, spatial details are tightly resolved in the two images. The numerous patch reefs located north of the central lagoon are shown in more detail as well as the numerous line reefs inside the atoll. Although both images generally produced effective bathymetric charts, some limitations still exist.

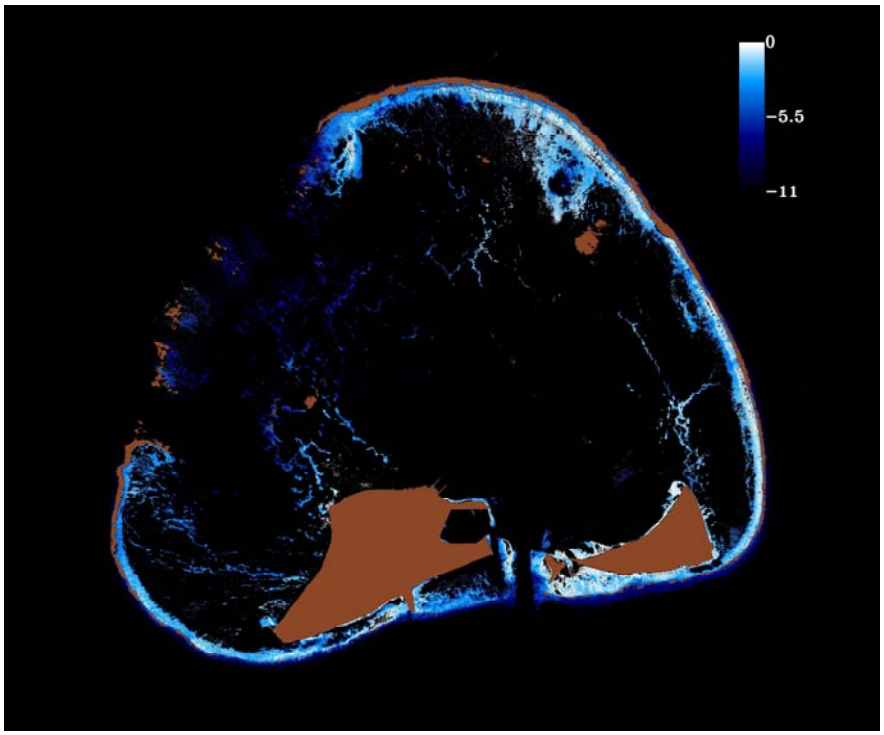

Figure 29. QuickBird derived bathymetry for Midway Atoll using the ratio method applied the coral/algae class. Depths are shown in meters. The brown regions are land, cloud, and breaking waves in the atoll's rim.

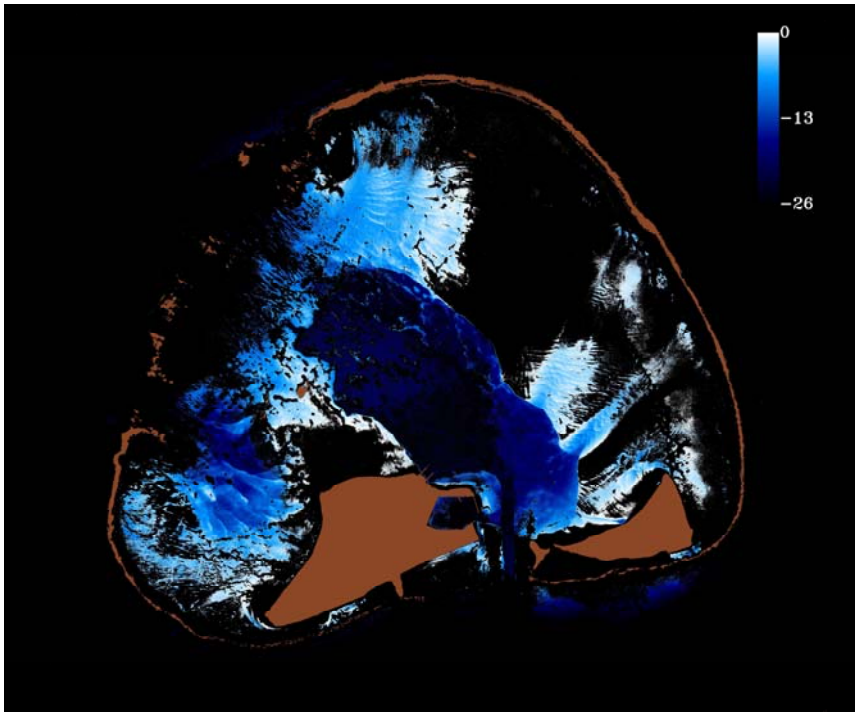

Figure 30. QuickBird derived bathymetry for Midway Atoll using the ratio method applied to sand classes. Depths are shown in meters. The brown regions are land, cloud, and breaking wave's in the atoll's rim.

Both images produced erroneous, underestimated results over very shallow sand areas. This error occurred in water depths of less then 2m and mainly over the bright sand in the eastern potion of the atoll and on the back reef. In the coral/algae class bathymetry (Figure 29), approximately 11% of the total number of pixels in the scene contained erroneous depth values. Their distribution was mostly confined to areas of less than 1m in depth (about 8% of the pixels) so an offset of 1m was applied to the image to correct for this. The sand bathymetry image (Figure 30) produced erroneous (underestimated) depths values over shallow bright sand. Additionally, masks were applied to both images to the dark water pixels of the open ocean area surrounding the atoll where the water is too deep for the algorithm to perform successfully.

The depth range derived from the sand subset is 0-26m (Figure 30). The deep portions of the lagoon in this subsetted image match the nautical chart soundings more accurately. The coral/algae class yielded a depth range of 0-11m (Figure 29).

C. COMPARISON BETWEEN IMAGES

For the accuracy assessment, a limited choice of sounding reference data exists for Midway Atoll: the only available reference was the nautical chart of Midway Atoll (Chart No. 19482, scale 1:10,000). Due to the finite amount of time available to carry out the *in situ* surveys, and the fact that the surveys ended up with a bias for shallower depths, the *in situ* data was used only for training purposes, and could not be used for accuracy assessment purposes as well. The derived bathymetry was thus compared to soundings from the nautical chart. In terms of overall accuracy, the ratio method applied over variable bottom types produced improved results when compared to the entire image bathymetry, although the improvement is marginal. The accuracy was tested using 25 soundings from the nautical chart of Midway Atoll (a higher number of reference soundings from the nautical chart could not be used for the reasons outlined in Chapter V). Thirteen points were collected from the sand class and 12 points from coral/algae class. The predicted depths were correlated with the chart soundings as a measure of accuracy. The correlation coefficients indicated that both methods yielded good results (> 80% accuracy). The correlation coefficient obtained using the ratio method over the entire image is 82% (Figure 31) compared to 86% (Figure 32) when the ratio method was applied over variable substrates. It must be noted that the small improvement was achieved using only limited field data and reference (nautical chart) data and using only two main bottom types.

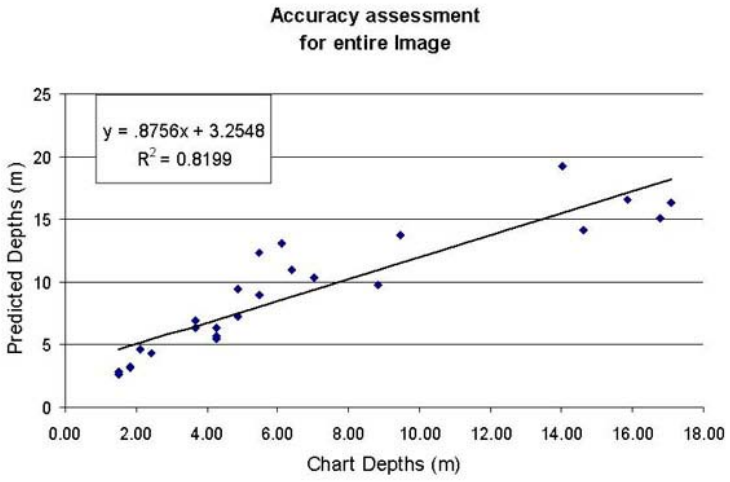

Figure 31. The absolute bathymetry when regressed against the chart depth explains 82% of the variation around the mean.

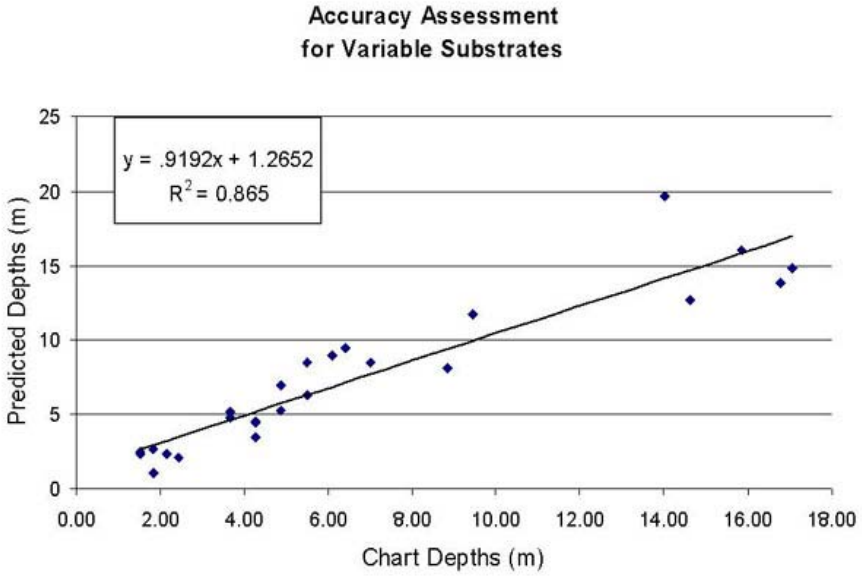

Figure 32. The absolute bathymetry when regressed against the chart depth explains 86% of the variation around the mean.

A direct comparison of the images in the depth range of shallow (< 2m) to intermediate and deep water (5-15m) revealed the average difference between predicted and chart depths ranged between 1.5 to 3m using the ratio algorithm over the entire scene. The accuracy was improved to .65 to 2m using the ratio method over variable substrates.

Both bathymetric outputs (entire image and variable substrates) generated erroneous depth values over the bright sandy regions in less than 2m of water depth. Additionally, both methods generally produced greater depths in deeper areas than those reported on the Midway nautical chart, although this was not quantitatively assessed. This is most likely caused by the paucity of field data used to tune the coefficients rather than by poor performance of the algorithm, discussed in the following section.

THIS PAGE INTENTIONALLY LEFT BLANK

VII. DISCUSSION

The bathymetry derived by pre-classifying the scene and tuning the coefficients separately for each bottom type represents an improvement over the original method described in Stumpf et al. (2003). This research demonstrated both the effectiveness of the algorithm to map remote benthic environments, as well as the improvements to the current ratio algorithm when applied separately over variable substrates. It also pointed out limitations of the algorithm not addresses by its authors. The ratio algorithm performed well using limited soundings, which demonstrates the resourcefulness of this method when applied to extensive areas such as Midway Atoll, with limited *a priori* data. Additionally, the hypothesis that the ratio method described by Stumpf et al. (2003) is improved by tuning the coefficients for the algorithm separately for each bottom type was here proved correct, although the difference, given that the data available for this study, was not statistically significant. Finally, this study confirmed limitations in the ratio algorithm for deriving depth values over areas of high reflectance in very shallow waters.

A good correlation of 82% was obtained between predicted depth and actual depths from a nautical chart over the entire image. This result is remarkable given the limited number of *in situ* surveys when the total area encompassed by the atoll is taken into consideration. Using merely 25 training points from a combination of field surveys and nautical soundings to tune the algorithms coefficients, a bathymetric file was produced that identified major coral structures, patch reefs, and the wide range in depth across the atoll. Features shallower than 20 meters were mapped with good accuracy. Reticulate reef areas near the center of the lagoon are clearly discernable, as well as the multiple depth changes around the reefs and sand chutes surrounding the reefs. The numerous patch and line reefs throughout the atoll are also mapped with relative accuracy. If the number of training points could have been increased (from 25 to 60, for example), the accuracy of the bathymetry would be greatly increased.

Inclusion of bottom type information to tune the ratio algorithm improved the overall map accuracy in both vertical and horizontal detail. A correlation of 86.5% was obtained by tuning the coefficients separately, resulting in an improved accuracy

compared to the entire image bathymetry, although the difference cannot be deemed statistically significant. Key benthic features are clearly reproduced, such as the pinnacle and patch reefs in northern lagoon area. Sand ripples caused by wind generated waves are clearly mapped throughout the image. Additionally, the algorithm was reliable in retrieving features at greater depths. Although it remains to be established if the retrieved absolute depths retain sufficient accuracy for navigational purposes, the analysis presented here demonstrate that the ratio method is a valuable tool to augment bathymetric information on remote coral reef locations.

Although the method proved a sound technique to derive water depth in coral reef environments, several limitations become apparent with this research. One such limitation is the algorithm's inability to produce accurate depth values in very shallow areas characterized by high reflectance values. The algorithm failed to produce depths over the bright sand and coral located in less than 2m of depth. The high reflectance values caused the ratio algorithm to overestimate the depth values, which produced invalid results. This can be attributed to the high values of apparent reflectance in the green band. The algorithm places the green band in the denominator which causes the ratio method to produce results close to zero as albedo is increased. This limitation has been observed in other studies (Clark, 2005; Densham, 2005) and creates problems in locations with extensive shallow coral and sand. This problem was partially addressed by offsetting the overestimated image values. This was done assuming that they are linearly related to the rest of the image, which was deemed a realistic assumption by a quick comparison with nautical chart depths.

An important limitation in this research was the inadequate number of data points collected from the fieldwork completed at Midway Atoll. The survey campaigns for this research took considerable time and funding to complete. Despite collecting over 80 data points over a period of 12 days at Midway Atoll, the field data collected did not represent the normal distribution of the depth values at Midway Atoll. The Random Sampling pattern strategy devised prior to the field work ensured that all the habitats were surveyed, but could not account for depth range. This resulted in the groundtruth points being representative of all bottom types but biased toward shallower depths. A sufficient number of water depths were collected in shallow waters (<10m), but locations in the

deep portions of the lagoon and on the fore reef were not surveyed adequately (surveying deep sites means deeper dives, which increase the surface time interval required between dives, and therefore require more time to complete). In fact only a total of 6 dive sites were surveyed in water depths over 10m. This limited the range values available to calculate the regression coefficients. In an environment with multiple bottom types and depth variations, the standard error is amplified when limited data are collected. Other researchers have suggested that at least 150 or more field surveys should be conducted to perform supervised classifications and accuracy assessments (Mumby, 2002; McCoy, 2005; Congelton, 1999), and this number increases with increasing area. Finally, this limitation in groundtruth data also prevented a thorough accuracy assessment. McCoy (2005) and Congelton (1999) suggest dividing the field data in 2 sets: the training dataset and the accuracy assessment dataset. In this study this was not possible because the deeper depth values collected in the field needed to be used in the training dataset.

To summarize, many possible sources of error affect the accuracy of the bathymetric derivation presented in this study. Although merging similar classes from the benthic classification and creating two main bottom types allowed bathymetry derivation over variable substrates that produced improved results, some classes of the original classification (Figure 20) had to be omitted, because they lacked sufficient groundtruth data. Although the depth values produced in this research are a good indicator of the actual bathymetry inside the atoll, future research or fieldwork is needed to fine tune the results and carry out a more extensive accuracy assessment.

A limited amount of groundtruth points with respect to the area studied (> 100 km^2) made it necessary to augment the field data with soundings from a nautical chart for both training and assessing the bathymetry. Since no other depth reference, such as LiDAR, was available for Midway Atoll, the nautical chart depths were assumed sufficiently accurate, even though the nautical charts from this region were found to contain inaccuracies during fieldwork carried out by other researchers since 2000 (Siciliano, pers. comm.). Additionally, soundings were obtained from the chart by the traditional method of using compass and ruler. This simple method made it difficult to locate the exact point on the chart and on the digital image was difficult. To compensate for possible geospatial error between the chart and digital QuickBird image, soundings

were selected over areas that encompassed major, recognizable structures, such as large patch reefs, and uniform areas of constant depth.

As mentioned, another potential source of error was the application of an offset due to the algorithm's failure over very shallow areas with high albedo. The offset was applied by examining the Gaussian distribution of the overestimated depth values, omitting the tail end on the distribution.

An important consideration for bathymetry derivation with spectral imagery is the cost and time required for the collection of an appropriate number of data points in the field. Today any algorithm available for bathymetry derivation requires field data to scale relative bathymetry to absolute values. Therefore, groundtruth work remains an important element of remote sensing analyses. Remote locations, such as Midway Atoll, require several days of transit to reach the destination. Unlike other remote atolls, Midway Atoll has an active runway, which greatly facilitates access and reduces travel time: other locations, such as the neighboring Kure Atoll or many other atolls in the central Pacific, are only accessible by ship, making this kind of work more difficult and expensive. Additionally, any *in situ* assessments carried out on SCUBA ideally require experienced divers and some knowledge of marine environments, particularly, in this case, coral reef environments. Our field team lacked extensive diving experience and had little or no prior knowledge of underwater environments, which inevitably slowed down the fieldwork process. Even though the team completed numerous surveys, the groundtruth data was scarce when compared to the extensive area (> 100km^2) encompassed by the atoll's environments. Moreover, typical weather and sea constraints further reduced the efficiency of field surveys. Ideally, either more personnel or more time in the field would be required. Furthermore, the travel cost to remote locations is usually high and cost constraints may prevent other research teams from collecting adequate field data to complete studies in remote locations.

VIII. CONCLUSION AND RECOMMENDATIONS

The effectiveness of Stumpf et al. (2003) ratio method to resolve bathymetry with the ability to tune the coefficients with limited soundings demonstrate its resourcefulness. The results in this research indicate that improved bathymetric mapping can be obtained by subdividing the scene into its different bottom types and tuning the algorithm's coefficients separately for each substrate. The ratio method applied to the entire scene produced accurate depth results with most major vertical features and depth variations represented. Improved results were obtained by pre-classifying the imagery into its main bottom types. Features over low-albedo substrates, such as coral and algae, were represented with greater accuracy. Additionally, sand substrates showed improved depth accuracy throughout the atoll. This demonstrates that Stumpf et al. (2003)'s algorithm does not implicitly compensate for variable bottom type and albedo as was originally concluded by its authors and postulated by Clark (2005).

The study also confirmed the inability of Stumpf et al. (2003) ratio method to perform well over shallow, high albedo substrates, such as sand in waters less than 2m in depth. The algorithm consistently failed in those areas. This limitation has been previously reported by other researchers, including Mumby (2004) and Clark (2005).

There are numerous opportunities for improvements on the work presented here. In order to conduct a thorough accuracy assessment of the methods described in this paper, additional field data would have to be collected in deep waters inside and outside the atoll, unless an overflight with a system retrieving high accuracy depth, such as the LiDAR sensor become available. LiDAR data could then be used as the reference dataset as in the study by Clark (2005). A cost-benefit analysis for collecting *in situ* data in remote areas could also be useful. Most importantly, new research should focus on resolving the algorithm's inability to estimate accurate depths over shallow areas with high albedo.

THIS PAGE INTENTIONALLY LEFT BLANK

APPENDIX A. QUICKBIRD METADATA FILE

```
version = "Q";
generationTime = 2004-12-13T18:02:01.000000Z;
productOrderId = "000000174939_01_P001";
imageDescriptor = "Basic1B";
bandId = "Multi";
panSharpenAlgorithm = "None";
numRows = 7470;
numColumns = 6876;
productLevel = "LV1B";
radiometricLevel = "Corrected";
bitsPerPixel = 16;
compressionType = "None";
BEGIN_GROUP = BAND_B
      ULLon = -177.46451323;
      ULLat =   28.29090703;
      ULHAE =    -1.00;
      URLon = -177.29454635;
      URLat =   28.29004530;
      URHAE =    -1.00;
      LRLon = -177.29576290;
      LRLat =   28.12599775;
      LRHAE =    -1.00;
      LLLon = -177.46542684;
      LLLat =   28.12693010;
      LLHAE =    -1.00;
      absCalFactor = 1.604120e-02;
END_GROUP = BAND_B
BEGIN_GROUP = BAND_G
      ULLon = -177.46451323;
      ULLat =   28.29090703;
      ULHAE =    -1.00;
      URLon = -177.29454635;
      URLat =   28.29004530;
      URHAE =    -1.00;
      LRLon = -177.29576290;
      LRLat =   28.12599775;
      LRHAE =    -1.00;
      LLLon = -177.46542684;
      LLLat =   28.12693010;
      LLHAE =    -1.00;
      absCalFactor = 1.438470e-02;
END_GROUP = BAND_G
BEGIN_GROUP = BAND_R
      ULLon = -177.46451323;
      ULLat =   28.29090703;
      ULHAE =    -1.00;
      URLon = -177.29454635;
      URLat =   28.29004530;
      URHAE =    -1.00;
      LRLon = -177.29576290;
      LRLat =   28.12599775;
      LRHAE =    -1.00;
      LLLon = -177.46542684;
```

```
      LLLat =   28.12693010;
      LLHAE =    -1.00;
      absCalFactor = 1.267350e-02;
END_GROUP = BAND_R
BEGIN_GROUP = BAND_N
      ULLon = -177.46451323;
      ULLat =   28.29090703;
      ULHAE =    -1.00;
      URLon = -177.29454635;
      URLat =   28.29004530;
      URHAE =    -1.00;
      LRLon = -177.29576290;
      LRLat =   28.12599775;
      LRHAE =    -1.00;
      LLLon = -177.46542684;
      LLLat =   28.12693010;
      LLHAE =    -1.00;
      absCalFactor = 1.542420e-02;
END_GROUP = BAND_N
outputFormat = "NITF";
BEGIN_GROUP = IMAGE_1
      satId = "QB02";
      CatId = "1010010003527201";
      SceneID = "1";
      TLCTime = 2004-10-12T22:34:39.565507Z;
      numTLC = 2;
      TLCList = (
      (0,  0.000000),
      (7470,  4.330435) );
      firstLineTime = 2004-10-12T22:34:39.565507Z;
      avgLineRate = 1725.00;
      exposureDuration = 0.00057971;
      collectedRowGSD =   2.434;
      collectedColGSD =   2.425;
      meanCollectedGSD =   2.430;
      rowUncertainty =   34.00;
      colUncertainty =   34.02;
      sunAz = 155.4;
      sunEl =  51.2;
      satAz = 113.5;
      satEl =  89.3;
      inTrackViewAngle =  -0.0;
      crossTrackViewAngle =   0.6;
      offNadirViewAngle =   0.6;
      cloudCover =   0.1;
      PNIIRS = 3.0;
      imageQuality = "Excellent";
      resamplingKernel = "CC";
      TDILevel = 13;
      positionKnowledgeSrc = "R";
      attitudeKnowledgeSrc = "R";
      revNumber = 16775;
END_GROUP = IMAGE_1
END;
```

APPENDIX B. CLASSIFICATION GUIDE

DATE: _____ **TIME:** _____ **DIVE/SNORKEL #:** _____ **GPS coords:** _____
Dive dist. and bearing from boat: _____ **Photos #:** _____ **Depth:** _____

REEF HABITAT CLASSIFICATION FRAMEWORK FOR MIDWAY ATOLL, NWHI

ATOLL ZONES (select all that apply)	REEF HABITATS (select all that apply)	
A. LAND modifiers bare, vegetated ponds artificial (seawall, paving, bldgs., docks, etc.)	*GEOMORPHIC:* modifiers 1. calcareous pavement- 2. simple patch reef- 3. complex patch reefs- 4. linear reef- 5. pinnacle reef- 6. hole or pool- 7. vertical wall- 8. spurs and grooves- 9. pass or channel- 10. secondary islet, rocks, seastack, etc.)	*BOTTOM COVER:* ecological modifiers a. unconsolidated sediments- *mud, sand, rubble, cobbles, boulders, etc.)* b. hard bottom (other than live coral) c. submerged vegetation- turf algae macro (fleshy) algae- calcareous or coralline algae- d. live coral- *mixed* *monospecific* *massive* *encrusting* e. other invertebrates- sea urchins, sponges f. artificial- concrete, marine debris, metal, wood,
B. SHORELINE -INTERTIDAL modifiers sand/unconsolidated, artificial consolidated, tidepools		
C. REEF CREST (atolls, barrier reefs)		
D. FORE REEF		
E. SHELF- TERRACE		
F. DEEP ESCARPMENT		
G. LAGOON		
H. BACK REEF		
I. REEF TOP (submerged reef)		
Bottom cover abundance rating: D = Dominant	A = Abund C = Comm O = Occasional	R = Rare

THIS PAGE INTENTIONALLY LEFT BLANK

LIST OF REFERENCES

Avery, T.E., and Berlin, G.L. 1992. Fundementals of Remote Sensing and Airphoto Interpretation. Macmillan Publishing Company, New York, NY.

Barton, I.J. 1995. Satellite derived sea-surface temperatures: current status. Journal of Geophysical Research. 100: 8777–8790.

Benny, A.H., and G.J. Dawson. 1983. Satellite imagery as an aid to bathymetric charting of the Red Sea. The Cartographic Journal. 20 (1): 5–16.

Bushuev, A.V., and A.V. Turchin. 1991. Operational use of sea ice remote sensing tools to support navigation in the Arctic and Antarctic. Geoscience and Remote Sensing Symposium, 1991. IGARSS '91. Remote Sensing: Global Monitoring for Earth Management. International, 797.

Chauhan, P., and S. Nayak. 2005. Detection of submerged reef banks in the Lakshadweep Sea using IRS-P4 OCM satellite data. Current Science. 89: 557–560.

Clark, R. E. 2005. Naval satellite bathymetry: A performance assessment. Master's Thesis, Naval Postgraduate School, Monterey, California.

Congalton, R.G., Green, K. 1999. Assessing the accuracy of remotely sensed data: principles and practices. Boca Raton, Florida. Lewis Publishers.

Densham, M. 2005. Bathymetric Mapping with QuickBird data. Master's Thesis, Naval Postgraduate School, Monterey, California.

Digital Globe, Inc. 2004. QuickBird Imagery Products: Product Guide. Longmont, Colorado: Digital Globe, Inc.

Digital Globe, Inc., K. Krause. 2003. Radiance Conversion of Quickbird Data. Longmont, Colorado: Digital Globe, Inc.

Digital Globe, Inc., K. Krause. 2005. Radiometric use of QuickBird Imagery. Longmont, Colorado: Digital Globe, Inc.

Doxaran, D., Nagur, C., and S.J. Lavendar. 2006. Apparent and inherent optical properties of turbid estuarine waters: measurements, empirical quantification relationships, and modeling. Applied Optics. 45 (10): 2310–2324.

Duntley, S.Q. 1963. Light in the Sea. Journal of the Optical Society of America, 53: 214–233.

Eilperin, J. 2006. Hawaiian Marine Reserve to be Worlds Largest. Retrieved August 10, 2006, from the Washington Post Web site: http://www.washingtonpost.com/wp-dyn/content/article/2006/06/14/AR2006061402455.html

Fisher, T.M. 1999. Shallow water bathymetry at Lake Tahoe from AVIRIS data. Master's Thesis, Naval Postgraduate School, Monterey, California.

Green, E.P, Mumby, P.J., Edwards A.J., Clark, C.D., (Ed. A.J. Edwards). 2000. Remote sensing handbook for tropical coastal management. Coastal Management Sourcebooks 3, UNESCO, Paris.

Hedely, J.D., Harborne, A.R., and P.J. Mumby. 2005. Simple and robust removal of sun glint for mapping shallow-water benthos. International Journal of Remote Sensing. 26 (1, part 2): 2107–2112.

Hochberg, E.J., Adrefouet, S., and M.R. Tyler. 2003. Sea surface correction of high special resolution IKONOS images to improve bottom mapping in near-shore environments. IEEE Transactions on Geoscience and Remote Sensing. 41 (7): 1724–1729.

Jenson, J.R. 2000. Remote Sensing of Water. Retrieved August 10, 2006, from the University of South Carolina Web site: www.cas.sc.edu/geog/rslab/551/Lectures/Chapter11_Water.ppt

Jerlov, N.G. 1976. Marine Optics. Elsevier, Amsterdam.

Jupp, D.L.P. 1988. Background and extensions to depth of penetration (DOP) mapping in shallow coastal waters. Proceedings of the Symposium on Remote Sensing of the Coastal Zone, Queensland, September 1988, IV2.1–IV2.29.

Kirk, J.T.O. 1994. Light and Photosynthesis in Aquatic Ecosystems. Cambridge University Press, Cambridge.

Kogan, F.M. 2001. Operational space technology for global vegetation assessment. Bulletin of the American Meteorological Society. 82: 1949–1964.

Leica Geosystems Geospatial Imaging, LCC. 2006. ATCOR for IMAGINE 9.0. Norcross, GA.

Lillesand, T.M., Kiefer, R.W. and J.W. Chipman. 2004. Remote Sensing and Image Interpretation. New York: JohnWiley and Sons, Inc.

Louchard, E. M., Reid, P. R., Stephens, C. F., Davis, C.O., Leathers, R. A., and V.T. Downes. 2003. Optical remote sensing of benthic habitats and bathymetry in coastal environments at Lee Stocking Island, Bahamas: A comparative spectral classification approach. Limnology and Oceanography. 48 (1, part 2): 511–521.

Lubin, D., W. Li, P. Dustan, C. Maxel, and K. Stamnes. 2001. Spectral signatures of coral reefs: Features from space. Remote Sensing of the Environment. 75: 127–137.

Lyzenga, D. R. 1978. Passive remote sensing techniques for mapping water depth and bottom features. Applied Optics. 17 (3): 379–383.

Lyzenga, D. R. 1981. Remote sensing of bottom reflectance and water attenuation parameters in shallow water using aircraft and Landsat data. International Journal of Remote Sensing. 1: 71–82.

Lyzenga, D. R. 1985. Shallow-water bathymetry using combined lidar and passive multispectral scanner data. International Journal of Remote Sensing. 6 (1): 115–125.

Maragos JE, Potts DC, Aeby GA, Gulko D, Kenyon J, Siciliano D, and D. VanRavenswaay. 2004. 2000–2002 Rapid Ecological Assessment of Corals (Anthozoa) on Shallow Reefs of the Northwestern Hawaiian Islands. Part 1: Species and Distribution. Pacific Science 58(2): 211–230.

Maritorena, S., A. Morel, and B. Gentili. 1994. Diffuse reflectance of oceanic shallow waters: Influence of water depth and bottom albedo. Limnology and Oceanography. 39 (7): 1689–1703.

Martin, S. 2004. An Introduction to Ocean Remote Sensing. Cambridge, UK: Cambridge University Press.

McCoy, R.M. 2005. Field Methods in Remote Sensing. New York: The Guildford Press.

Mishra, D.R., Narumalani, S., Rundquist, D., and M. Lawson. 2005. Characterizing the vertical diffuse attenuation coefficient for downwelling irradiance in coastal waters: Implications for water penetration by high resolution satellite data. Photogrammetry and Remote Sensing. 60: 48–64.

Mobley, C.D.1994. Light and Water: Radiative Transfer in Natural Waters. Academic Press, San Diego.

Morel, A., Prieur, L. 1977. Analysis of variations of ocean color. Limnology and Oceanography. 22 (4): 709–722.

Morris, K. 2005. Midway Atoll: National Wildlife Refuge and Battle of Midway National Memorial. [Pamphlet]. U.S. Fish and Wildlife Serive.

Mumby, P., Clark, C., Green, E., and A. Edwards. 1998. Benefits of water column correction and contextual editing for mapping coral reefs. International Journal of Remote Sensing. 19 (1): 203–210.

Mumby, P.J., and A.J. Edwards. 2002. Mapping marine environments with IKONOS imagery: enhanced spatial resolution can deliver greater thematic accuracy. Remote Sensing of Environment. 82 (2): 248–257.

Mumby, P.J., Skirving, W., Strong, A.E., Hardy, J.T., LeDrew, E.F., Hochberg, E.J., Stumpf, R.P., and L.T. David. 2004. Remote Sensing of coral reefs and their physical environment. Marine Pollution Bulletin. 48: 219–228.

Olsen, R.C. 2006. Remote Sensing from Air and Space. In press, SPIE.

Philpot, W. D. 1989. Bathymetric mapping with passive multispectral imagery. Applied Optics. 28 (8): 1569–1578.

Polcyn, F.C., and D.R. Lyzenga. 1973. Calculations of water depth from ERTS-MSS data. Proceedings, Symposium on significant results from ERTS-1, NASA Spec. Publ. SP-327.

Prasert, S. 2005. Multi angle imaging with spectral remote sensing for science classification. Master's Thesis, Naval Postgraduate School, Monterey, California.

Research Systems, Inc. 2004. ENVI Tutorials. Boulder, Colorado: Research Systems, Inc.

Robinson, I.S. 2004. Measuring the Oceans from Space. Chichester, UK: Praxis Publishing LTD.

Rosenshein, J.S., Goodwin, C.R., and A. Jurado. 1977. Bottom configuration and environment of Tampa Bay. Photogrammetry and Remote Sensing. 43: 693.

Short, N.M. 2006. The remote sensing tutorial. Retrieved August 10, 2006, from the National Aeronautics and Space Administration Web site: http://rst.gsfc.nasa.gov/

Siciliano, D. 2005. Latitudinal limits to coral reef accretion: testing the Darwin point hypothesis at Kure Atoll, Northwestern Hawaiian Islands, using new evidence from high resolution remote sensing and in-situ data. Doctoral Dissertation, University of California Santa Cruz, 2005.

Smith, R. C., and K. S. Baker. 1981. Optical properties of the clearest natural waters. Applied Optics. 20 (2): 177–184.

Stuffle, L.D. 1996. Bathymetry from hyperspectral imagery. Master's Thesis. Naval Postgraduate School, Monterey, California.

Stumpf, R.P., Holderied, K., and M. Sinclair. 2003. Determination of water depth with high-resolution satellite imagery over variable bottom depths. Limnology and Oceanography. 48 (1, part 2): 547–556.

Tewinkel, G.G. 1963. Water depths from aerial photographs. Photogrammetry and Remote Sensing. 29: 1037.

Thomas, G.E. and K. Stamnes. 1999. Radiative Transfer in the Atmosphere and Ocean. Cambridge, UK: Cambridge University Press.

Weidmark, W.C., Jain, S.C., Zwick, H.H., and J.R. Miller. 1981. Passive bathymetric measurements in the Bruce Peninsula. In: Proceedings, Fifteen International Symposium on Remote Sensing of the Environment. Environmental Research Institute of Michigan, Ann Arbor.

Zhongping, L., Kendell, L. C., Mobley, C.D., Steward, R.G., and J.S. Patch. 1999. Hyperspectral remote sensing for shallow waters: Deriving bottom depths and water properties by optimization. Applied Optics. 38 (18): 3831–3843.

THIS PAGE INTENTIONALLY LEFT BLANK

INITIAL DISTRIBUTION LIST

1. Defense Technical Information Center
   Ft. Belvoir, Virginia

2. Dudley Knox Library
   Naval Postgraduate School
   Monterey, California

3. Dr. Richard C. Olsen. Code PH OS
   Naval Postgraduate School
   Monterey, California

4. Dr. Daria Siciliano, Code PH
   Naval Postgraduate School
   Monterey, California

5. Angela Puetz, Code PH
   Naval Postgraduate School
   Monterey, California

6. Barry Christenson
   U.S. Fish and Wildlife Service
   Honolulu, Hawaii

7. John Klavitter
   U.S. Fish and Wildlife Service
   Honolulu, Hawaii